Mariana Pereira Tomé

Bachelor of Science in Micro and Nanotechnologies Engineering

Ni-Foil etching to improve the adhesion of carbon electrodes and enhance supercapacitor performance

Dissertation submitted in partial fulfillment of the requirements for the degree of Masters in Micro and Nano-technologies Engineering

Orientador:	Dr. Kush K. Upadhyay, Post doctoral researcher, C2C-NewCap
Co-orientadores:	Prof. Luís Miguel Nunes Pereira, Associate Professor, DCM, FCT-UNL

Júri

Chairperson:	Prof. Rodrigo Ferrão de Paiva Martins, Full Professor, DCM, FCT-UNL
Raporteur:	Dr. João Carlos Mesquita Coelho, Doctoral Researcher, DCM, FCT-UNL
Member:	Dr. Kush K. Upadhyay, Post doctoral researcher, C2C-New Cap

July 2021

FACULDADE DE CIÊNCIAS E TECNOLOGIA
UNIVERSIDADE NOVA DE LISBOA

Ni-Foil etching to improve the adhesion of carbon electrodes and enhance supercapacitor performance

ACKNOWLEDGMENTS

Em primeiro lugar, um agradecimento à Faculdade de Ciências e Tecnologias da Universidade NOVA de Lisboa. Em especial, ao Prof. Dr. Rodrigo Martins e à Prof. Dra. Elvira Fortunato por serem os grandes impulsionadores do curso que dou agora por concluído.

I would like to express my most heartfelt gratitude to my supervisor, Kush, for helping me on this path. Your availability, interest, and knowledge will always prevail as something I look up to. Also, thank you for always motivating me to do better.

Ao meu coorientador, Professor Luís Pereira, deixo o meu agradecimento por me ter permitido realizar esta tese e por me proporcionar todas as condições para realizar a mesma.

A todas as pessoas no CENIMAT e CEMOP que de uma maneira ou outra estiveram envolvidas no meu percurso, muito obrigada. Em especial, ao Tomás Calmeiro pela ajuda no AFM e ao Tiago Carvalho, por sempre me ter ajudado e pela disponibilidade, interesse e conhecimentos.

To all the C2C- New Cap team, for giving me the privilege of doing the thesis in a place where every day I learned something new. To a team filled with people always willing to help, advise, teach, whom I respect very much and express my sincere gratitude.

A nível mais pessoal, não posso deixar de agradecer á minha família. Aos meus pais, por tudo. À minha irmã, a quem agradeço por estar sempre do meu lado. Pelo conforto que é ter as minhas sobrinhas na minha vida. À minha tia Lurdes e tio Zé, por estarem sempre presentes e por todo o carinho. E à minha avó.

Ao Gui, por todo o apoio, companhia, amor e amparo sempre. Muito obrigada.

A todos os meus amigos pela companhia nos momentos de estudo e de lazer, que me permitiram chegar à tese. À Moniz e à Raquel, pela companhia nas infinitas horas de estudo, e ainda mais pela companhia nas horas de almoço, café, lanche, jantar, boleias, etc., sempre mais proveitosas que as horas de estudo. A todos os habitantes daquela rua do Serrado, os que lá viviam e os que lá conviviam. Ao Madeira (também por todos os momentos no tico), Rui, Zé, Carvalho, Dmytro, Gui, Diogo Patrício, Diogo Lopes, Edu, Nia, Margarida, Leonor, Kika e Tomás. Por todos os momentos inesquecíveis que passámos na faculdade e fora dela, muito obrigada. À minha afilhada, por ser brutal. A todos que partilharam a experiência de ERASMUS comigo, gracias chicos/chicas!

A quem vem desde antes da faculdade e seguirá depois da mesma. À Lucy, por tudo e mais alguma coisa. À Raquel, Rafa e Drica, por todos os momentos divertidos que passámos, seja sob o sol alentejano ou sob a chuva da Amadora. Ao Lameiras, por termos crescido juntos.

RESUMO

A investigação na área do armazenamento e conversão de energia tem sido crescente ao longo dos últimos anos. Devido ao esforço constante para um mundo cada vez mais sustentável, torna-se importante fornecer sistemas de conversão de energia fiáveis e eficazes para inúmeras aplicações. Neste sentido, os supercondensadores têm tido uma extensa investigação, permitindo que sejam vistos como uma alternativa para substituir baterias em tecnologias como o arranque de motor, entre outras.

Os materiais para a construção destes dispositivos estão exaustivamente estudados na literatura. No entanto, processos como as técnicas de revestimento e as técnicas associadas à montagem dos dispositivos necessitam de ser aprofundados para a produção a uma larga escala. Um passo crítico no aumento da escala são os pré-tratamentos que são feitos nos substratos (coletor de corrente), para uma melhor adesão entre o material ativo e o substrato condutor, que por norma é uma superfície lisa. O objetivo deste trabalho foi, neste sentido, de aumentar a adesão da chapa de níquel ao material ativo.

Para tal, diferentes técnicas de *etching* foram aprofundadas. O *etching* químico foi estudado, obtendo a solução com a melhor performance e otimizando os parâmetros das diferentes soluções testadas. Processos complementares como a calandragem e o *screen-printing* foram também analisados. Para além disto, o *etching* físico foi estudado, otimizando os parâmetros usados. Os elétrodos produzidos através destas técnicas foram estudados através de SEM, AFM, ângulo de contacto, teste de corte transversal e análise eletroquímica.

A melhor performance foi obtida com a solução ácida $FeCl_3$ a 15% em água desionizada, que permitiu reduzir a resistência interfacial de 0.021Ω numa chapa de níquel limpa para 0.008Ω na amostra que sofreu o *etching*. Isto representa uma redução de 2.6 vezes. Para além disto, a capacitância aumentou em 51%, de 16.5F na chapa de níquel limpa para 25F na amostra que sofreu o *etching*.

Assim, este trabalho permitiu obter a melhor solução para aumentar a rugosidade da chapa de níquel. Foi também possível provar que o aumento da rugosidade leva a um aumento da performance do supercondensador, através da diminuição da resistência interfacial e aumento da capacitância.

Palavras-Chave: armazenamento de energia, supercondensadores, coletor de corrente, chapa de níquel, adesão, *etching*, resistência interfacial

ABSTRACT

A lot of research is being focused on the field of energy storage and conversion nowadays. It is very important to provide energy conversion and good storage systems for many applications. Batteries and supercapacitors are thus receiving a lot of attention. The past research on supercapacitors allowed them to be widely seen as an alternative for high-power applications to replace batteries in technologies as important as UPS, car regenerative breaking, and engine starting.

Literature highlights a vast range of potential materials but scarcely addresses the scaling-up manufacturing process of supercapacitors. A critical step during manufacturing is substrate pre-treatments, required for adequate adhesion of the active material on the conductive substrate, that tends to be smooth with low roughness. In this thesis, etching techniques on nickel foil substrate have been tested to increase the surface roughness and improve the adhesion.

For this purpose, different etching techniques were studied. Chemical etching solutions were considered, obtaining the best performing one and optimizing the etching parameters for the studied etchant solutions. Complementary to this, techniques like screen-printing and calendaring were also performed and tested with the chemical etching. Also, dry etching was studied aiming to optimize its parameters. The performance of these etched electrodes was evaluated through techniques as diverse as SEM, AFM, contact angle, cross-cut test, and electrochemical analysis. The best performance was achieved with the acidic solution $FeCl_3$ at 15% in DI water, reducing the interfacial resistance from 0.021Ω in a clean nickel foil substrate to 0.008Ω in an etched sample, making it 2.6 times smaller and thus proving that this etching increased the adhesion. Furthermore, there was also a 51% increase in capacitance, from 16.5F to 25F in the etched sample over 2000 cycles.

Overall, this work allowed to obtain the best etchant to increase the roughness of the nickel foil. This roughness increase proved to enhance the supercapacitor performance, diminishing the ESR and increasing the capacitance.

Keywords: energy storage, supercapacitors, current collectors, nickel foil, adhesion, etching, ESR.

TABLE OF CONTENTS

LIST OF TABLES

LIST OF FIGURES

SYMBOLS

µm – micrometer

A - Ampers

Al – Aluminium

Ar – Argon

cm – centimeter

Cu – Copper

F – Farad

Hz – Hertz

Ni – Nickel

m – meter

M – Molar

min – minutes

mm – Millimeter

mL – Milliliter

mTorr – Militorr

nm – nanometer

s – seconds

S – Siemens

scmm – standard cubir centimenter per minute

Ti – Titanium

V – Volts

W – Watts

Kg – kilogram

°C - Degrees Celsius

Ω - ohm

ACRONYMS

AFM – Atomic force microscopy

CC – Current collector

CD – Charge-discharge

CV – Cyclic voltammetry

CE – Counter electrode

CPE – Constant phase element

DI – Deionized

ED – Energy density

EDS – Energy dispersive spectroscopy

ESS – Electrochemical energy storage

EIS – Electrochemical impedance spectroscopy

EDLC – Electric double layer capacitor

ESS – Energy storage systems

ESR – Equivalent series resistance

IHP – Inner Helmoltz plate

ISO – International standardization organization

Li-ion- Lithium-ion

OHP – Outer Helmoltz plate

OCP – Open circuit potential

RE – Reference electrode

RMS – Root mean square

SEM – Scanning electron microscopy

SCE – Saturated calomel electrode

SC – Supercapacitor

USD – United States dollar

UPS – Uninterrupted power supply

UV – Ultraviolet

WE – Working electrode

MOTIVATION AND OBJECTIVES

The uncontrolled usage of fossil fuels over the last decades has increasingly contributed to the energy crisis, causing surmounting visible environmental problems never seen before. Therefore, it is of utmost necessity to develop and investigate efficient ways not only to harness energy from renewable sources but also to store them in efficient and robust ways that will consequently propel stable economic growth and technological evolution [1, 2].

The efforts towards a switch from the use of fossil fuels to renewable energy are already being actively done, as can be seen in **Figure 1**[3]. Today, 26% of the world's electricity is harnessed from renewable energy and is expected to reach 30%, at the increment rate of 1% each year, by 2024 as stated by the International Energy Agency (IEA). These transformations will lead to a substantial reduction in the use of hazardous raw materials and in the quest to find green and sustainable replacements [4]. It will also accelerate the aim towards reaching carbon neutrality by 2060, as proposed in the Paris agreement. The main drawback that comes with the benefits of renewable sources of energy is its intermittent availability in nature. These drawbacks can be overcome by developing reliable, efficient, and robust energy storage systems (ESS) whose applications range from storing renewable energy to the demanding electrification of vehicles [1].

The most commonly used and growing technologies related to ESS are batteries and supercapacitors (SC). Batteries are the most dominant technology in the market and are still expected to grow at an annual growth rate of over 12,31% until 2025[5,6]. However, supercapacitors have also started to gain a significant market share. Its market was valued at USD 887 million in 2020 and is expected to rise up to USD 1.869 million by 2026 [5]. This is mainly because of its advantageous properties such as high-power delivery rate, longer cycle life, improved safety, and low environmental concerns in contrast to batteries [7,8]. Nonetheless, its low energy density (ED) still requires improvement along with reduction in production costs. There are several possible ways proposed in literature to improve the ED. The most prominent one is to improve the specific surface area of the active material [9]. It is important to have a high specific surface area but more importantly, the active material should have good adhesion to the current collector to boost both energy density as well as power delivery rate. Better adhesion also minimizes the equivalent series resistance (ESR) and thereby improves the power delivery rate along with improved cycle life.

For that reason, this thesis work aims to improve the adhesion of the active material, in this case, activated carbon, to the Nickel foil (Ni-foil) current collector. To accomplish the goal, different etching techniques were applied to increase the roughness of the plain current collector surface.

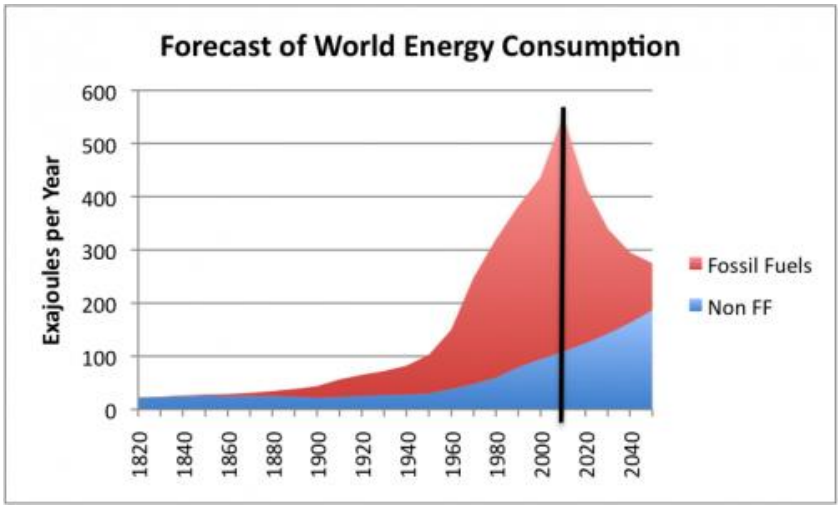

Figure 1 *- World energy consumption of fossil fuel and non-fossil fuels [10].*

1 INTRODUCTION

It is predicted that two-thirds of the total energy supply will be achieved from renewables by 2050 [10]. This shift has led to exponential advances in the technological developments of energy storage [11, 12]. This section provides a brief introduction to the different ESS and the importance of the adhesion of active material to the current collector.

1.1 TYPES OF ENERGY STORAGE DEVICES

Energy storage systems (ESS) are capable of storing and converting the energy in different forms. The stored energy can be further used depending on the required applications [13]. The types of energy storage devices will be detailed in the this sections [14, 15].

Electrochemical and electrostatic energy systems are mainly composed of batteries, capacitors, and supercapacitors. These can be further divided into others that will be detailed throughout this work. The Ragone plot which describes the power *vs.* energy characteristic properties of different devices is demonstrated in **Figure 2a)**, showing the differences in their energy storage capabilities and power delivery rate. These differences originate mainly from the mechanism involved in the charge storage processes [16].

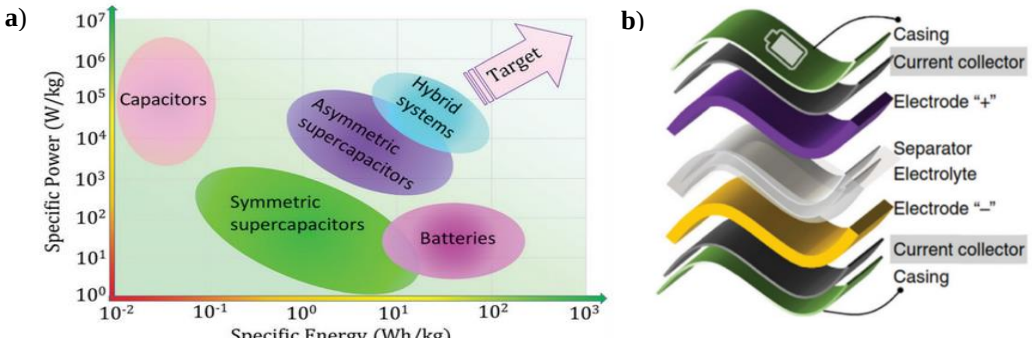

***Figure 2**- a) Ragone plot with specific power vs. specific energy of the above-mentioned energy storage devices; b) components of a typical energy storage device. Retrieved from [12]*

1.1.1 Batteries

Batteries convert electricity into chemical energy. They are generally composed of an anode and cathode separated by ion conducting polymeric separator immersed in suitable electrolyte [15, 17, 18]. The chemical reactions responsible for energy storage in these systems happen in the entire bulk of the material and thereby they possess high energy density. However, these benefits bring other challenges such as their limited rate performance, low power capabilities, and short cycle life, highlighted in **Table 1** [19, 20].

Li-ion batteries are the most studied and researched among the battery types. However, they have serious shortcomings such as the use of flammable and toxic organic electrolytes, recycling scheme, and high cost [21].

Another type of battery widely used is the lead-acid battery. These batteries are not environmentally desirable, given that lead is a toxic heavy metal that can contaminate and damage ecosystems [22, 23]. Nevertheless, they still occupy a large segment in the market and are indispensable in many applications, mostly due to its low cost.

1.1.2 Electrolytic capacitors

Unlike batteries, in electrolytic capacitors, the charge storage process is purely physical. These devices are composed of two parallel plates (usually metals) and a dielectric in between that acts as an insulator. The capacitance obtained with capacitors is in the range of pico to millifarads per device [12]. Supercapacitors, on the other hand, can elevate the properties of conventional capacitors and can achieve much higher capacitances [7].

1.1.3 Electrochemical capacitors

The beginning of the research on electrochemical capacitors, or commonly named supercapacitors (SC) dates back to 1957 and was first marketed in 1978 [24]. However, these devices have gained more attention recently. They can either complement or even replace batteries in many applications for example in hybrid vehicles, where SCs can be implemented to provide fast acceleration or to recover energy from kinetic energy when the vehicle breaks [25, 26].

Supercapacitors have a similar architecture to batteries. They have a positive and negative electrode, electrolyte, separator, current collector, and casing (**Figure 2b**) [27, 28]. A table with the main differences between SC and batteries is shown below. Within eletrochemcial capacitors, there are different types of devices, according to its charge storage mehcanism that will be detailed bellow.

***Table 1**- Comparison of different parameters for supercapacitors and batteries* [12, 29, 30]

Parameter	***Supercapacitor***	***Batteries***
Charge storage mechanisms	Surface based redox reactions/ EDLC	Chemical (faradaic)
Kinetics	Moderate to fast (for hybrid SC)	Slow to fast
Energy density (Wh kg^{-1})	1 to 10	20 to 150
Power delivered (W kg^{-1})	500-10000	<1000
Cycle-life	>10 years	Around 3 years
Operating voltage determined by	Cell/Electrode stability	Thermodynamics
Safety	Yes	No
Operating temperature (°C)	-40 to +85	-20 to +65
Cost	€€€	€

i. **Electrical double layer capacitor (EDLC)**

In these devices, the charge is stored via physical adsorption-desorption of oppositely charged electrolyte ions at the electrode/electrolyte interface, forming a double layer upon an applied potential (**Figure 3a**). The double layer is formed by a first layer due to the migration of ions into the inner electrode material – the inner Helmholtz plate (IHP) and the second layer is formed once the counter-ions in the electrolyte are attracted– outer Helmholtz plate (OHP)[31,32].

ii. **Pseudocapacitor**

The prefix *pseudo*, in these devices, relates to the fact that these materials share most of the characteristics of a conventional capacitive electrode (the charge stored is linearly dependent on applied potential), but its charge storage mechanisms are not like EDLC. In pseudocapacitors, the charge storage originates from electron-transfer mechanisms (fast and successive redox reactions) [33,34], which increase the capacitance. The reactions that take place in pseudocapacitors are mainly surface-based redox reactions (very fast kinetics) [35] or intercalation type reactions (electrolyte intercalates into tunnels or layers) [36].

***Table 2** - Main advantages and disadvantages of a hybrid supercapacitor compared to a traditional EDLC* [40–42]

EDLC	***Hybrid supercapacitor***	***Pseudocapacitor***
Higher cycle-life	Higher ESR (Equivalent Series Resistance)	Lower power density
High power density	Cannot be discharged to 0 V	Lower cycle life
Temperature independent	Higher energy density	Higher energy density
Reversible	Linear discharge profile	Higher capacitance
Fast Kinetics	Higher capacitance	-
-	Higher operating voltage	-

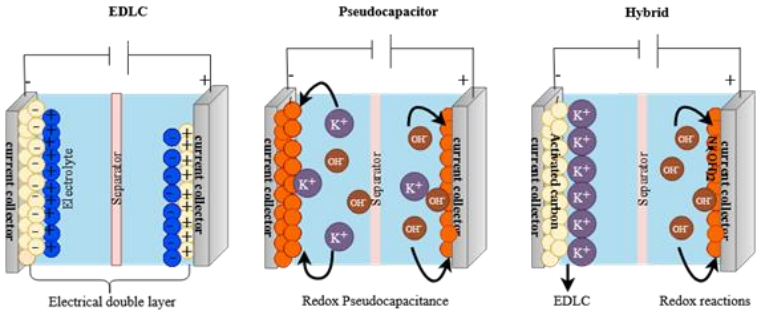

***Figure 3**- Types of SC: a) EDLC, b) Pseudocapacitor and c) hybrid device (with the materials that are implemented in this work).*

According to its structure, these devices can also be further dividied into symmetric and asymmetric devices.

a) Symmetric devices

In these devices, both electrodes share the same charge storage mechanism- eletric double-layer capacitance. The electrode materials chosen in these devices should have high surface area, to accumulate as much charge as possible. Also, materials with an appropriate pore structure are advantageous as it facilitates the diffusion of electrolyte ions throughout the active material [7]. Carbon-based materials such as graphene and activated carbon are widely used [12].

b) Asymmetric (hybrid) devices

Asymmetric (hybrid) supercapacitors are devices that combine both moderate energy and high power (typical in supercapacitors) [12]. The first patent related to hybrid devices surfaced in the mid-'90s [33].

As can be seen in **Figure 3c**, in hybrid devices, two electrodes possessing different charge storage mechanisms are combined. In one electrode it stores similarly to EDLC and in the other, it stores similar to the faradaic redox reactions [29]. **Table 2** demonstrates the main characteristic differences among them. Hybrid supercapacitors have thus shown to have better performance compared to EDLCs but still require some improvements [37–39]. One example of a hybrid device is a setup of activated carbon as a negative electrode and $Ni(OH)_2$ as a positive electrode and this setup will be used as the basis of all electrochemical tests in this thesis [33].

1.2 STUDY OF THE CURRENT COLLECTOR (CC)

The continuous pursuit for an enhancement in the hybrid SC properties has led to a thorough study in recent years on its components (electrode, electrolyte, separator, and current collector). Lukatskaya, M. et al proposed the elimination of the current collector (CC) using free-standing electrodes[27]. However, this approach requires different materials with highly conductive properties (such as MXenes). The preparation of these materials has a very high cost associated and for that reason, the work on improving the CC surface is another approach just as important. The nature of the CC which holds the active material also plays a critical role in improving the charge storage performance. The surface modification of CCs is a practical and effective approach to improve the SC performance [43].

The main function of the current collector is to provide a link between the supercapacitor's active material and its external terminals and to provide support to the active material [44]. The electroactive material/current collector is a critical interface that plays a very important role in the electrochemical performance and cycle stability [45], as some studies have already proved [47,48]. Since the electrochemical processes take place at the surface of the active material, it is important to have a CC that is effective and that has good contact with the active material. If the adhesion strength to the active material is not optimized, delamination can occur, thus resulting in capacity loss, increased ohmic resistance, and lower cycle-life [45,49]. The ideal CC should possess, depending on its application:

(a) High electronic conductivity

(b) low contact resistance with the active material
(c) strong bonding with the electrode material
(d) inert towards the electrolyte
(e) high surface area per unit volume and mass
(f) high mechanical flexibility
(g) lightweight
(h) high thermal stability
(i) environmentally friendly
(j) low cost. [48,50]

The design of the CC to fit applications for flexible supercapacitors is also very important, although this is not the focus of this work. The study of these properties and consequent refinement decreases the overall resistance of the device and helps to enable high power which is of prime concern [48,51].

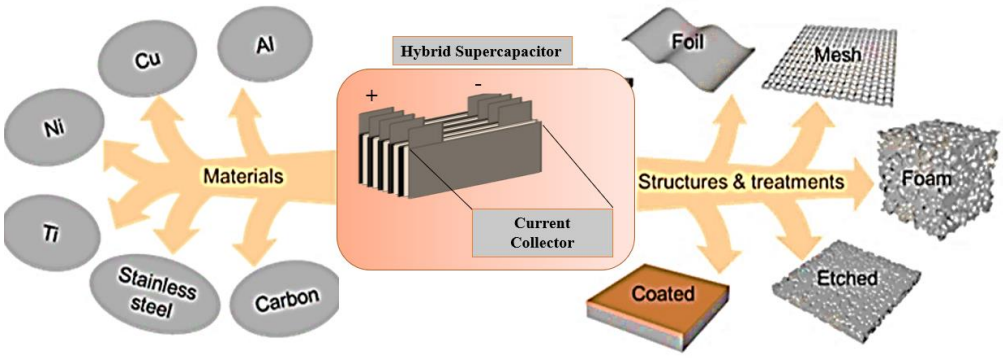

***Figure 4**- Materials and treatments done in current collectors. Adapted from [63]*

1.2.1 Metal foil-based current collectors

Metal foils are generally used as the CC because of their low price compared to other CCs used (such as mesh and others illustrated in **Figure 4**, recyclability, and its inertness towards the electrolyte, and its high electrical conductivity [51]. Foil materials such as nickel, aluminium, and copper have high electrical conductivity, desirable for these applications. From the above-mentioned CCs, nickel foil is widely studied at the academic as well as an industrial level[52]. However, the main challenge associated with it is its high interfacial resistance compared to metal foams [48,53].

The porous nature of metal foams provides an even distribution of the active material inside the current collector, therefore increasing the contact area and consequently decreasing the contact resistance. On the other hand, in metal foils, the current collector only exists on the back of the electrode material and therefore the whole material does not participate in the charge transportation (less contact area), which increases the contact resistance. Since the primary characteristics considered for current collectors are, among others, high electrical conductivity and low contact resistance it is very important to find methods to decrease the contact resistance in metal foils [47].

In the next section, the techniques employed in this work and other possible techniques are enlightened.

1.3 ETCHING TECHNIQUES TO IMPROVE THE ADHESION OF CC/ACTIVE MATERIAL

It is well studied and reported that a good adhesion (through more contact points) can eliminate the delamination of active material, for example, carbon from the current collector, and can enhance the electrochemical performance [45,57]. There are many technologies available to increase the adhesion property. In this thesis, we have targeted improving it through roughening the surfaces by using chemical etching. It was achieved by following two different approaches:1) through direct etching of the Ni-foil in different etching solutions and 2) by doing a selective etching on a pattern adequately created. The etching solution was tuned

depending on the nature of the current collector surface [55]. **Figure 5** shows the main outcomes and advantages of an etching treatment on the foil surface.

1.3.1 Chemical etching

A very well studied technique is wet chemical etching. Through this straightforward etching process, it is possible to obtain a rough surface with a high etch rate and relatively fast. However, there are also some problems associated. Wet chemical etching requires large amounts of acidic solutions for scale-up applications, and this limits the safety and convenience up to a certain extent. Furthermore, the etching solutions have to be constantly replaced to keep the same etching rate for different samples, increasing the costs and making the disposal scheme more troublesome [56]. Some of the factors that can affect the etching are time, temperature, stirring, etc. In this work, the nickel surface is roughened through chemical reactions that as a starting point form an oxide layer that then undergoes dissolution in a controlled way. These reactions will be further discussed in the results section [60,61]. Thus, it is very important to find an adequate etching solution that is both able to constantly form an oxide layer and then dissolve this layer to make the surface uniformly rough [59].

Literature highlights the favorable outcomes obtained from the chemical etching, and consequently an improved electrode performance. In some research works, it was possible to infer that etched CC improves the cycle stability and the cycle life of the device, with no apparent self-discharge [60].

1.3.2 Patterning techniques

Some techniques can be complementary to chemical etching. To achieve a surface that has an ideal adhesion with the active material coating, pores can be created on this surface with the purpose of making the active material particles fit perfectly in these pores. This can be obtained with printed techniques, that allow for a pattern to be created in the foil. Printing techniques are a promising field since they are compatible with fabrication at a wide range, the process is low cost, and its scale-up is relatively easy. Among these techniques, screen-printing is a widely used one. The resolution in screen-printing is limited to 50-150 μm, making it less suitable for its utilization for fine features [61]. In screen-printing, an ink is squeezed through a patterned screen and deposited onto the substrate. The quality of the procedure depends on the screen mesh, the printing parameters, the substrates, and the resin viscosity [62]. Other noticeable techniques emerging in the SC field are inkjet printing, roll-to-roll printing, among others [64,66,67].

1.3.3 Dry etching

Over the past few years, plasma processes have found increasing application for surface modification [55]. Plasma etching is a purely physical process, where the atoms or the molecules of the substrate are knocked out by kinetic energy[65]. Theoretically, this technique works in every substrate, making it appropriate for nickel etching [55]. Characteristics such as the capability for large-scale production, low material consumption, and the possibility to have good industrial hygiene (since it is performed in a vacuum chamber and the operator is not in contact with the reagents) make plasma etching very captivating. Notwithstanding, this technique is expensive, and the selectivity is very low, providing uneven results. Similar to plasma, lasers have been applied as a convenient technique to create surface patterns in current collectors [45,69]. The main limitation to scale up some of these processes is its high cost and environmental concerns. Besides, it is very important to take the promising results in SC cautiously, since the lab-scale is different from the commercialization [67].

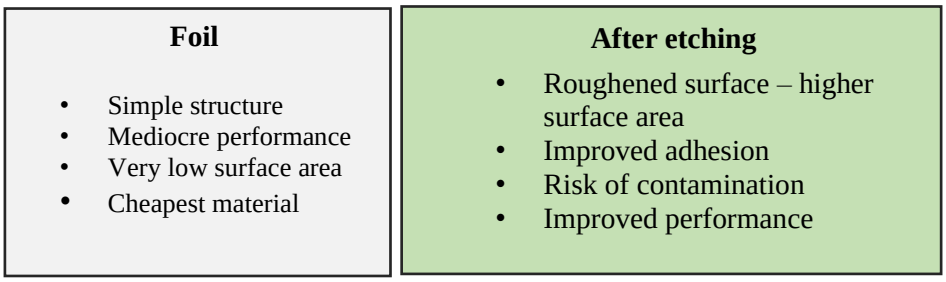

***Figure 5**- Main expected characteristics obtained after etching treatments on foil.*

2 MATERIALS AND METHODS

2.1 METAL FOIL PREPARATION

Commercial nickel foil with >99.6% purity and 50 µm of thickness was used. The foil roll was cut into small samples (8.5 × 11.5 cm^2). Prior to any experiment, the foil was cleaned using detergent followed by an ethanol bath and further dried at room temperature.

The steps taken for the sample preparation from the cleaning of Ni-foil to its etching and characterization are illustrated in the schematic presentation below, **Figure 6.** The schematic presentation shows that, after performing the etchings, the samples were either characterized (through SEM; AFM or contact angle) or were coated with the active material to go on to the electrochemical analysis in a 3-electrode setup and/or cross-cut test.

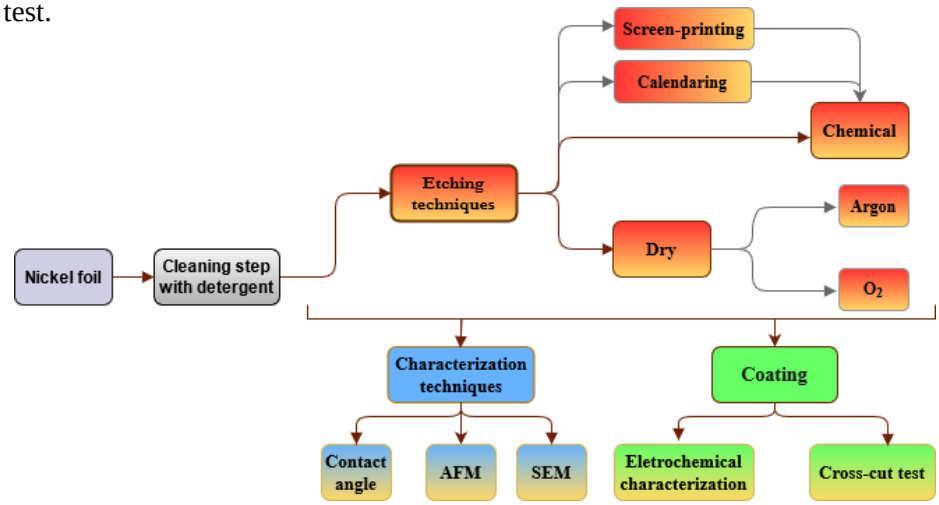

Figure 6- Schematic presentation of steps employed in this work.

2.2 CHEMICAL ETCHING

Several chemical etching solutions were studied, using varied periods of time (1-15 min) and temperature. The etching solutions composition, etching times, and other parameters are detailed in **Table 3**. The details of the reagents used can be found in the Annexes (**Table 14**).

Table 3- Etching solutions, preparation and parameters studied.

Etching solution	***Solution preparation***	***Etching parameters***
HCl/HNO_3 (Aqua regia) at 4:1 ratio	• Preparation of 300 mL. • Pour 60 mL of HNO_3 into a beaker; • Add 240 mL of HCl slowly; • Let the solution cool for 30 minutes before using.	• 3 minutes • 5 minutes • 10 minutes
$H_2SO_4/H_2O_2/H_2O$ (4:1:15)	• Preparation of 300 mL. • Pour 150 mL of DI water into a beaker; • Add 10 mL of H_2O_2; • Add 40 mL of H_2SO_4 slowly under constant stirring; • The reaction is exothermic, so it is important to let it cool down before using.	• 1 minute • 3 minutes • 5 minutes • 10 minutes • 15 minutes
($FeCl_3$) (Iron chloride) at 30% and 15%	• Preparation of 300 mL for 15% and 30%. • Pour the DI water into the beaker; • Add $FeCl_3$ to the DI water very slowly and stir for 10 minutes or until a homogeneous solution is obtained.	• 3 minutes • 5 minutes • 10 minutes • 40 °C • 50°C • 70°C

After each etching step, the samples were put in a DI water bath for 3 minutes followed by an ethanol bath for the next 3 minutes, and then dried at room temperature.

2.2.1 Screen-printing

Screen-printing was performed prior to the chemical etching. At first, the screen-printing step was performed using a resin resistant to the chosen chemical etching solution. Afterward, chemical etching was carried out following the process discussed in the previous section to etch the uncovered metal substrates and thus achieve the desired pattern. Based on the conclusion from the chemical etching experiments, which will be detailed in the Results section, $FeCl_3$ was used as the chemical etchant since it showed better electrochemical performance.

For the screen-printing process, the resin was composed of acrylic (TB 3003 K, ThreeBond), and titanium dioxide (TiO_2) nanoparticles (Rockwood) and was printed with the mask provided by CENIMAT-i3N (FCT-UNL) using a mesh, and then dried at 90°C for 20 minutes. The Ni-foil was patterned with two layers of resin to ensure the blockage of corrosive acidic solution to the covered part of the foil.

After masking, the samples were etched using 30% $FeCl_3$ at 70 °C for 5 minutes. Then the samples were cleaned in a DI water bath for 5 minutes and further dried at room temperature. As a final step, the resin was removed using an acetone bath where samples were kept for around 15 minutes.

To infer if the mask was well linked to the foil, images from the optical microscope were also taken (Zeiss Axioscope 5 optical microscope) and are displayed in **Figure 27**, in Annexes.

2.2.2 Calendaring

In this process, the Ni foil was first calendared and then the chemical etching was done. It was calendered placing the foil in between Nifoam sheets with two different gaps to obtain two different apparent roughnesses. A hot roller press machine available at C2C-NewCap was used for the calendaring purpose. Then the etching was done using $H_2SO_4/H_2O_2/H_2O$ and $FeCl_3$ as an etchant solution.

2.3 DRY ETCHING

Dry etching was done using plasma etching equipment (Trion Phantom 3 reactive ion etcher (RIE-ICP) available in CENIMAT-i3N (FCT-UNL)), which can be operated in CF_4, SF_6, Ar, and O_2 gaseous environments. Chemically etched foil was also used as a substrate for this etching to improve the roughness further. **Table 4** details the etching conditions.

Table 4- Conditions applied in dry etching

Target	***Gas***	**Flow rate (scmm)**	**Power (W)**	***Pressure (mTorr)***	***Time(min)***
Ni foil	Argon	15	250	20	30 min each side
Etched Ni foil	Argon	15	250	20	30 min each side
Ni foil	O_2	15	250	20	30 min each side
Etched Ni foil	O_2	15	250	20	30 min each side

2.4 CHARACTERIZATION TECHNIQUES

2.4.1 SEM

Morphological and compositional analyses were conducted using a field emission scanning electron microscope (FESEM-FIB, Carl Zeiss Auriga Crossbeam microscope) with energy dispersive X-ray spectroscopy (EDS, Oxford XMax 150). These tests were performed in CENIMAT-i3N (FCT-UNL).

2.4.2 AFM

The surface roughness of the electrode was obtained using an Asylum Research MFP-3D Standalone (Oxford Instruments). Topography was recorded. Images were exported using Gwyddion software. These tests were performed in CENIMAT-i3N (FCT-UNL).

2.4.3 Contact angle

The surface wettability was studied using contact angle (Dataphysics OCA15plus) according to the sessile drop method. These tests were performed in CENIMAT-i3N (FCT-UNL).

2.4.4 Cross-cut test

To evaluate the adhesion between the coating (done in section 2.4.1) and the etched current collector, a cross-cut tester (TQC CC2000 Cross Cut Adhesion Test KIT) with 2 mm teeth distance in the cutter was used. A scheme of the procedure applied is shown in **Figure 7**. The current collector/carbon coating interface adhesion was tested under two conditions: 1) with the dry electrode and 2) with the wet electrode after 10 days soaking in the used electrolyte **(Figure 7b**)). The set of rules to determine the adhesion strength using this equipment are provided in annexes (**Figure 28**). These tests were performed in C2C-New Cap.

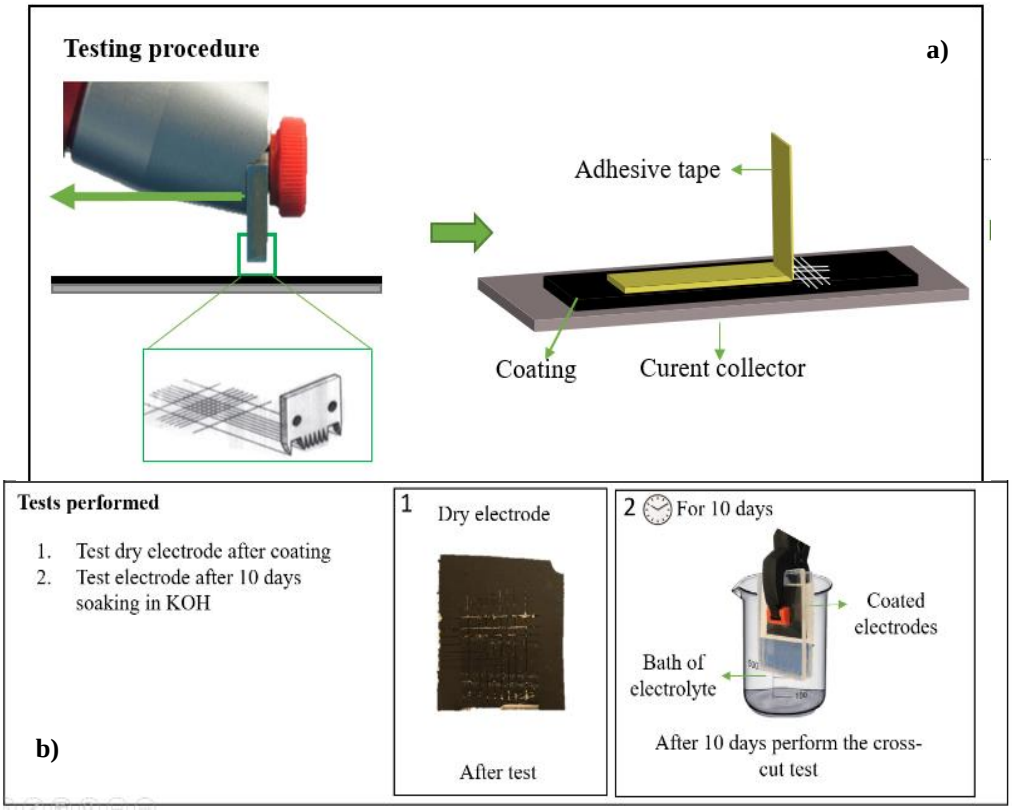

Figure 7- a) testing procedure for the crosscut test and b) parameters used for the tests performed.

2.5 ELECTROCHEMICAL ANALYSIS

2.5.1 Carbon coating process

All the treated and reference substrates were coated with a carbon slurry made using a C2C-New Cap formulation. After coating, the electrodes were dried in a convection oven at 80°C for 30 minutes. The average total thickness of the electrode with the coating was 100-125 µm. To proceed to the cell assembly, the coated substrates were cut with a size of 7×7,5cm^2.

The cells were then assembled using the carbon coated current collector where all the etching tests were performed as the working electrode and a $Ni(OH)_2$ electrode as the counter electrode separated by a polymeric separator. It was clamped properly to ensure the proper alignment of the electrodes. All the tests were done in 7 M KOH electrolyte.

Two different methods were used to evaluate the adhesion property: 1) electrochemical measurements and 2) through cross-cut tests.

2.5.2 Electrochemical testing procedure

The electrochemical analysis was performed in a 3-electrode setup to obtain an in-depth study of the active material and to have information on the individual electrode without interference from the electrochemistry of the other electrodes, in this case, the carbon adhesion to the current collector[26]. The measurement was performed in a 3-electrode setup in the *Gamry 5000E* potentiostat. The developed carbon electrode was used as the working electrode, nickel hydroxide as the counter electrode, and a saturated calomel electrode (SCE) as reference. It was decided to use the Nickel-based electrode (supplied by C2C) as a counter electrode to reduce the number of gas bubbles released by this electrode, which could interfere with the electrochemical experiments. The testing procedures are detailed in **Table 5.** The electrochemical analysis was performed in C2C-New Cap.

Table 5- Electrochemical testing procedure.

Testing procedure	***Testing parameters***	***Comments***
1) Electrochemical impedance spectroscopy (EIS)	At OCP in the frequency range of 100 KHz to 1 mHz	To obtain the interfacial resistance - ESR.
2) Cyclic voltammetry (CV)	In range of 0 to -1V at scan rates: 10, 30, 40, 50, 100 mV/s	0 to -1V is the obtained operating potential window
3) Conditioning	30 minutes at a fixed potential of -1.2V	Outside the operating potential window where the stability towards the materials is lower and thus the CC/activated carbon interface is less stable
4) EIS	Set fixed potential of -1.2V in the frequency range of 100 KHz to 1 mHz	To evaluate the ESR with the cell under fixed potential.
5) CV	In range of 0 to -1V at scan rate: 30 mV/s	To infer the decrease in performance (current) after the destabilization of the electrode due to conditioning outside the potential window. This plot should be compared to the one at the same scan rate from step 2)
6) Open circuit potential (OCP)	For 3 hours	To stabilize the cell
7) EIS	At OCP in the frequency range of 100KHz to 1mHz	To evaluate a possible increase in the resistance due to destabilization of the electrode.
8) Charge-Discharge (CD)	Only for the best performing cells. 2000 cycles	To check capacitance, cycle stability, and coulombic efficiency

3 RESULTS AND DISCUSSION

3.1 PHYSICO-CHEMICAL CHARACTERIZATION

The focus of this thesis was to improve the nickel foil/active material adhesion through roughening the nickel foil surface, i.e., increasing the surface area of the nickel foil. To that end, efforts were made to find the optimum etching conditions employing chemical, dry, and a mix of both chemical and dry etching. In this section, the Physico-chemical characterization of the different etched samples will be discussed, through SEM, AFM, and contact angle. Further, the cross-cut test results will also be detailed, to find the degree of adhesion of the active material to the current collector. Finally, the electrochemical analysis will also be presented and discussed to have a better understanding of the etching phenomena and resulting roughness.

3.1.1 Chemical and dry etching

All the etched samples were characterized through different tools detailed in the discussion section. Ni foil without any etching treatment was considered as the reference sample and is referred to as "Reference" in the document and used for comparison with other treated Ni foils. Ni foil with an adequate adhesion treatment provided by C2C is referred to as "Benchmark". In this work, the benchmark CC was evaluated to infer if the etchings performed could match this solution. As stated before, three different chemical etching solutions were employed in this work: HCl/HNO_3 (aqua regia) at 4:1 ratio; $H_2SO_4/H_2O_2/H_2O$ at 4:1:15 ratio and $FeCl_3$ at 15% and 30% concentration. **Figure 8** illustrates the etching process using aqua regia. On treating the Ni foil in the acidic solution (step 1 in **Figure 8**), at first, the nickel gets oxidized (step 2 in **Figure 8**) which further leads to the dissolution by forming the corresponding salts. As a result, the process makes the surface rougher (step 3 in **Figure 8**) [11]. Etching time and temperature were varied to obtain the optimum results. The results obtained from each solution are presented in this section.

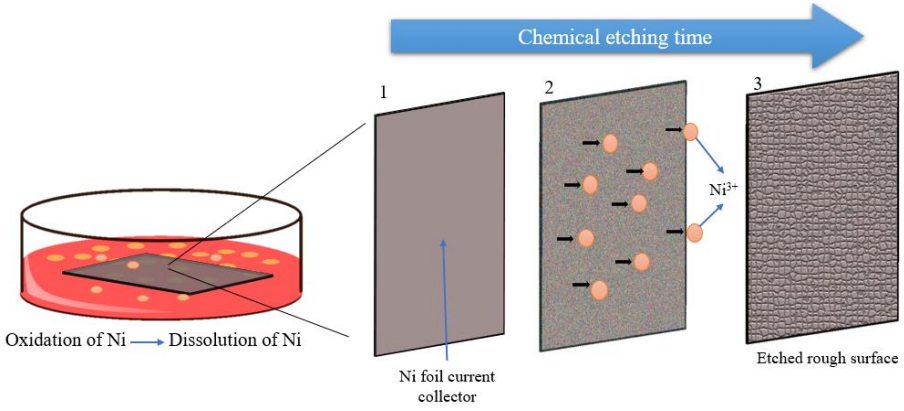

Figure 8- Schematic representation of chemical etching process using aqua regia.

i. **Characterization on Reference CC**

At first, the reference electrode was characterized to make a comparison with the treated CC. The resulting SEM analysis is presented in **Figure 9.** The reference image shows no apparent roughness at both magnifications (**Figure 9a&b)**, confirming that it is a flat surface. At higher magnifications, there appear to be some wrinkles in the foil.

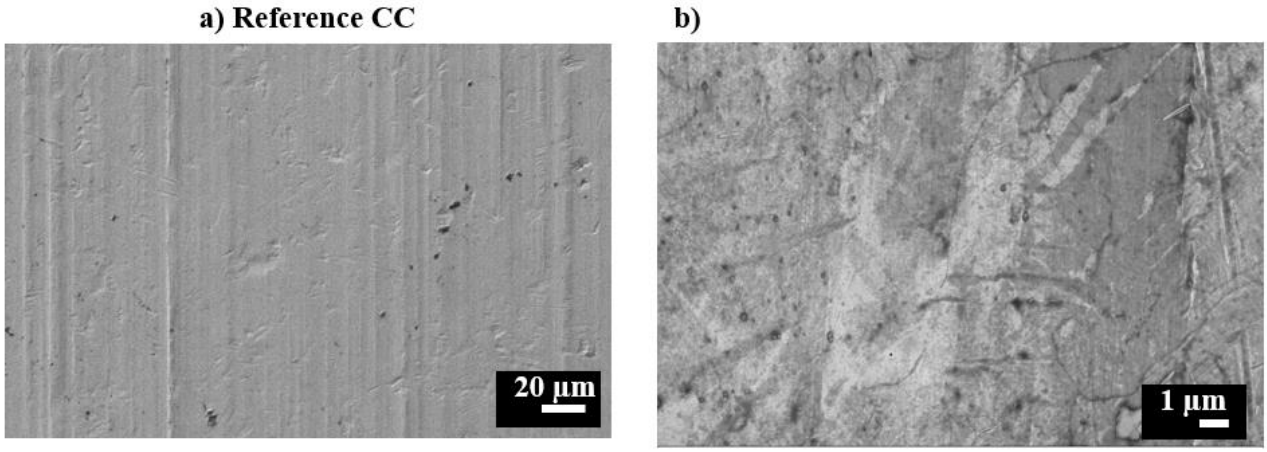

Figure 9 - SEM images of a & b) Reference CC at different magnifications.

ii. Characterization of HCl/HNO_3 (4:1) treated CC

The possible reactions on the Ni-surface on immersing in the acidic solution are given below [68–70],

$$Ni + NO_3^- + 4H^+ \leftrightharpoons Ni^{3+} + 2H_2O + NO \qquad (1.1)$$

$$Ni^{3+} + 4\,Cl^- \leftrightharpoons NiCl_4^- \qquad (1.2)$$

And the overall reaction

$$Ni + HNO_3 + 4HCl \leftrightharpoons HNiCl_4 + 2H_2O + NO \qquad (1.3)$$

In this acidic solution, HNO_3 acts as an oxidizer and oxidizes Ni following the reaction (1.1). In the subsequent step, the chloride ions (HCl) react with the oxidized Ni, reaction (1.2), to form a complex ion that dissolves nickel from the surface of the foil. In this study, the time was optimized to avoid too severe or too mild effects. The optimum time was **10 minutes** which was verified from cross-cut and electrochemical tests elaborated in the following section.

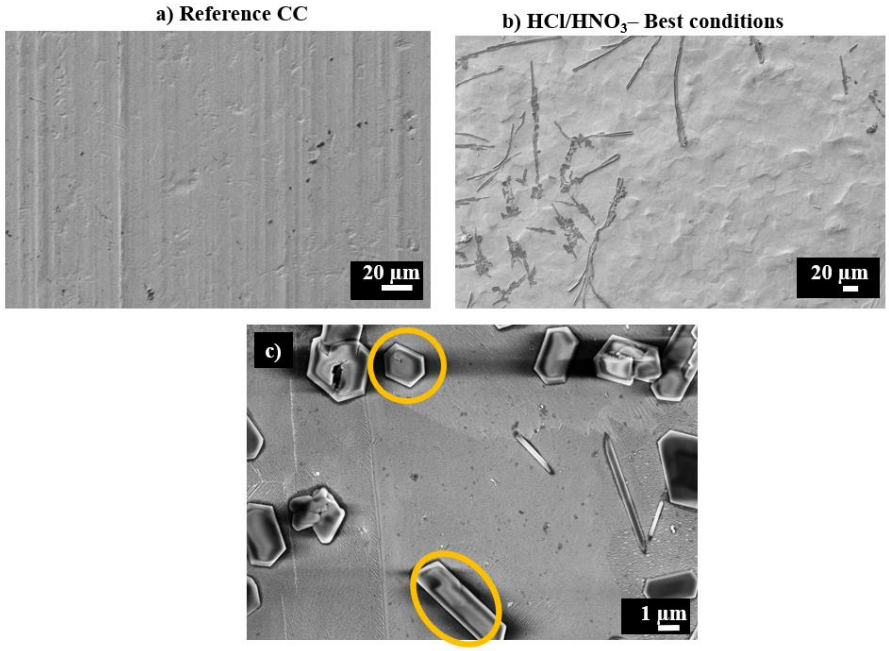

Figure 10- SEM images of a) reference CC and b &c) etched HCl/HNO_3 .

Figure 10 shows the SEM images on the reference current collector (**Figure 10a**) and the exposed sample to the aqua regia (**Figure 10b&c**). After immersed in the solution for the optimal time of 10 minutes, the

etching became visible at this magnification through some pits. However, this apparent roughness was not uniform on the surface. There was a slight improvement in the electrochemical performance, possibly due to the partial etching that occurred. The pits observed for this etching time could be attributed to a starting point of the complete nickel dissolution. These pits, circled in **Figure 10c**, have an apparent structure of crystallographic etched pits [71,72]. Therefore, this etchant solution seems to create sophisticated microstructures on the nickel foil. Upon increasing the etching time, the whole nickel surface started to dissolve vigorously making the foil very thin, which was not desired. These results also show that this solution leads to micro-scale modifications in the surface, owing to the more acidic character of the solution (stronger etching) [51]. Also, though etching occurred, the fact that it did not occur evenly along the surface could not enable an even anchoring in the current collector and therefore may negatively affect the adhesion. It is also important to note that this etching process requires proper handling and precautions as the solution used is very corrosive and its fumes are very hazardous. In addition, the etching activity of this solution diminishes after a short time and that could be a bottleneck in a scaled-up process. For these reasons, this solution was considered ineffective.

iii. **Characterization of $H_2SO_4/H_2O_2/H_2O$ (4:1:15) treated CC**

In this solution, hydrogen peroxide acts as an oxidizer following the reaction (2.1) and further undergoes dissolution in the presence of sulfuric acid by the reaction (2.2) [30,73]

$$\mathrm{Ni} + H_2O_2 \leftrightharpoons \mathrm{NiO} + \mathrm{H_2}O \qquad (2.1)$$

$$\mathrm{NiO} + H_2SO_4 \leftrightharpoons \mathrm{Ni}SO_4 + \mathrm{H_2}O \qquad (2.2)$$

The overall reaction involved can be given as

$$\mathrm{Ni} + H_2SO_4 + H_2O_2 \leftrightharpoons \mathrm{Ni}SO_4 + 2\mathrm{H_2}O \qquad (2.3)$$

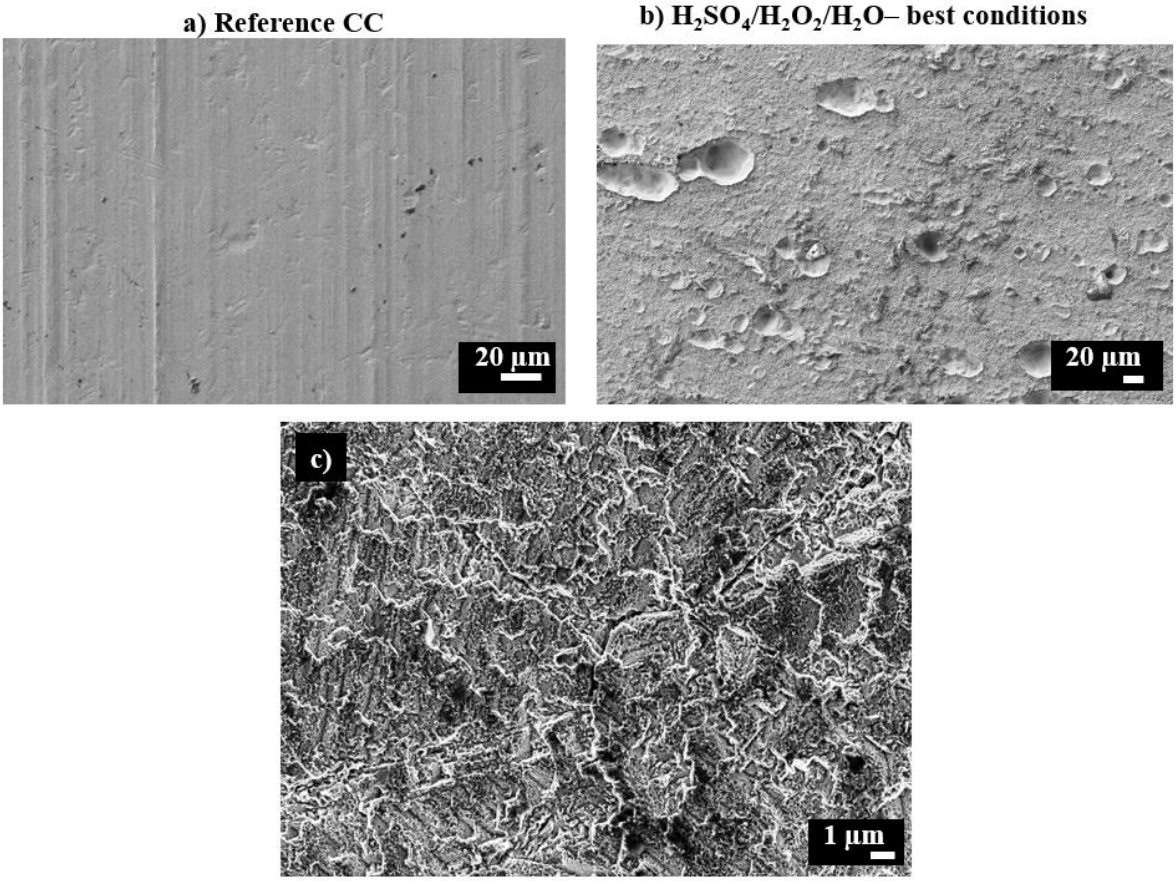

Figure 11 - SEM images of a) Reference CC and b-c) CC etched with $H_2SO_4/H_2O_2/H_2O$ at different magnifications.

The etching time was varied, and the optimal time obtained was **10 minutes**. The mass loss was not noticeable after the etching process indicating it was not as vigorous compared to the HCl/HNO_3 etchant solution. The SEM images of the etched and non-etched samples using this solution are demonstrated in **Figure**

11. The formation of a rougher surface after the etching is clearly evident in the form of irregularly shaped protrusions. The average size of the roughness created was calculated using *ImageJ* software and was around 12.2 µm, a wide mismatch from the carbon particles (5.7 µm-value provided by C2C). The "mountains" and "valleys" created are therefore oversized compared to the carbon particles. The etching rate does not seem to be the same, since, in **Figure 11b**, the formation of deeper valleys is visible. However, at higher magnification, the etching becomes more even on the surface. This sample has an increase in surface area at a higher magnification but at a lower magnification the increase does not seem to be as big, and this may lead to a non-optimal adhesion. The electrochemical analysis enabled to infer more conclusions regarding the effect of this etching in the adhesion.

iv. **Characterization of $FeCl_3$ (15%) treated sample**

This solution is composed of dissolved ferric chloride in water. The pH of this solution was typically lower than 7. In the etching process, at first, $FeCl_3$ oxidizes Ni which on further reaction leads to its dissolution as shown in the reactions (3.1) & (3.2), respectively [74-75] :

$$Fe Cl_3 + Ni \rightarrow Fe Cl_2 + NiCl \quad (3.1)$$

$$Fe Cl_3 + NiCl \rightarrow FeCl_2 + NiCl_2 \quad (3.2)$$

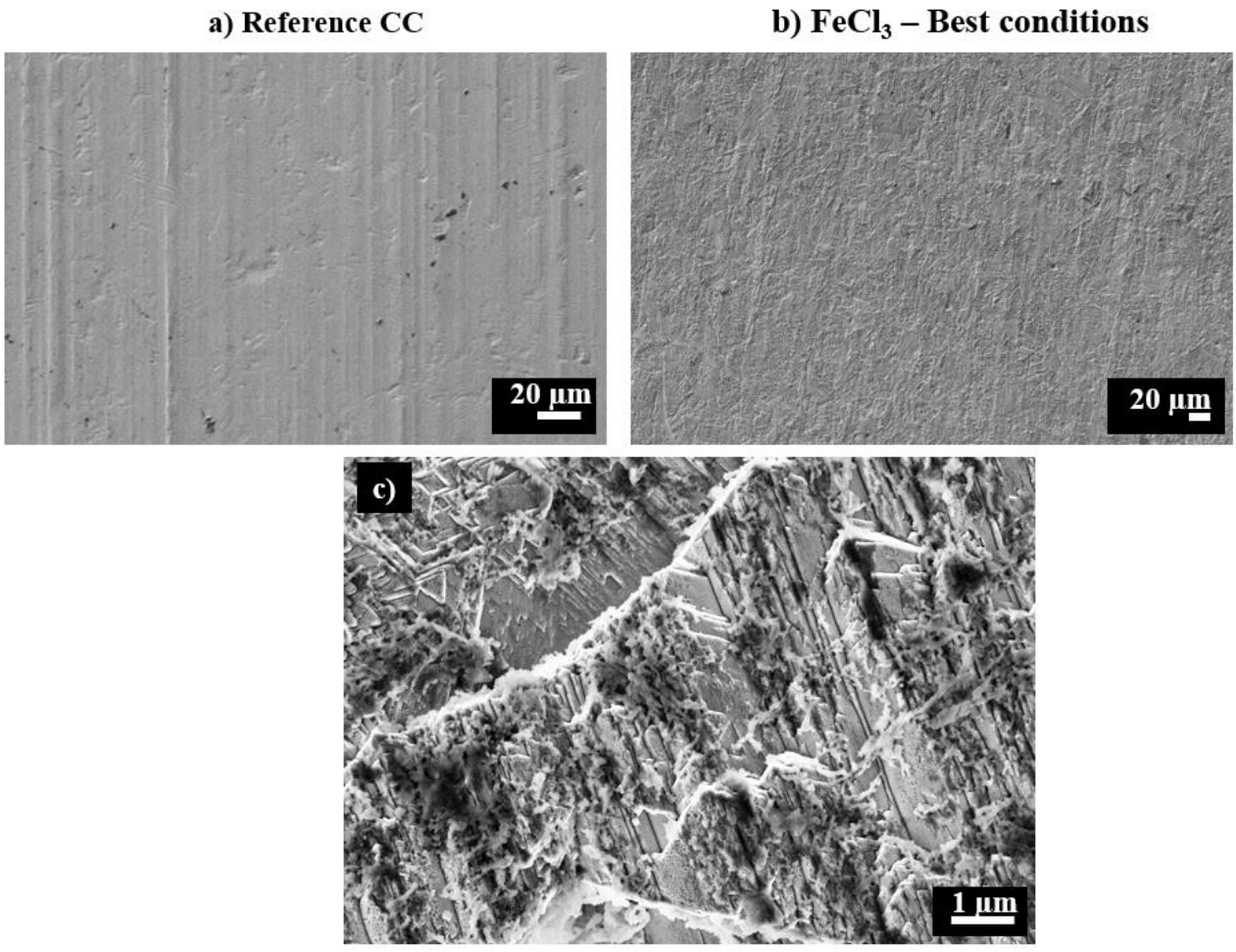

Figure 12- SEM images of a) Reference and b-c) Etched CC at different magnifications in $FeCl_3$ etchant.

The optimum parameter obtained using this etching solution was **15%** concentration at a temperature of **70 °C for 5 minutes**. This etching protocol is comparatively advantageous as it is a weaker acid and thus the scale-up process is expected to be simpler. The SEM image of this sample is illustrated in **Figure 12**. At lower magnification, it shows the etching has occurred uniformly throughout the exposed area (**Figure 12b**), and

also there was a significant increase in the surface area. In this study, there was a considerable loss in mass (almost 1g for the most aggressive conditions). This could represent a disadvantage given that the thickness of the CC should be optimal, otherwise there is a chance of increasing the ohmic resistance as well as breaking the foil. However, electrochemical results (detailed in section 3.4) evidenced no deterioration in the electrochemical performance. Theoretically, the increase in roughness increases the surface area [11]. When the slurry is then coated, a higher surface area offers more contact points and improves the adhesion strength. Therefore, the higher roughness in this etched foil can increase the surface area and offer more contact points. The roughness created was in the form of uniform protrusions with some surface step edges as visible in **Figure 12c**. In addition, the average microstructure size was 7.1 µm (shown in annexes, **Figure 29**) almost matching the used carbon particle size and satisfying the assumption that the roughness created would increase the adhesion by the effect of "trapping" the carbon particles tightly and thus enhance the adhesion strength.

The AFM measurements on etched CC using $FeCl_3$ etchant are below.

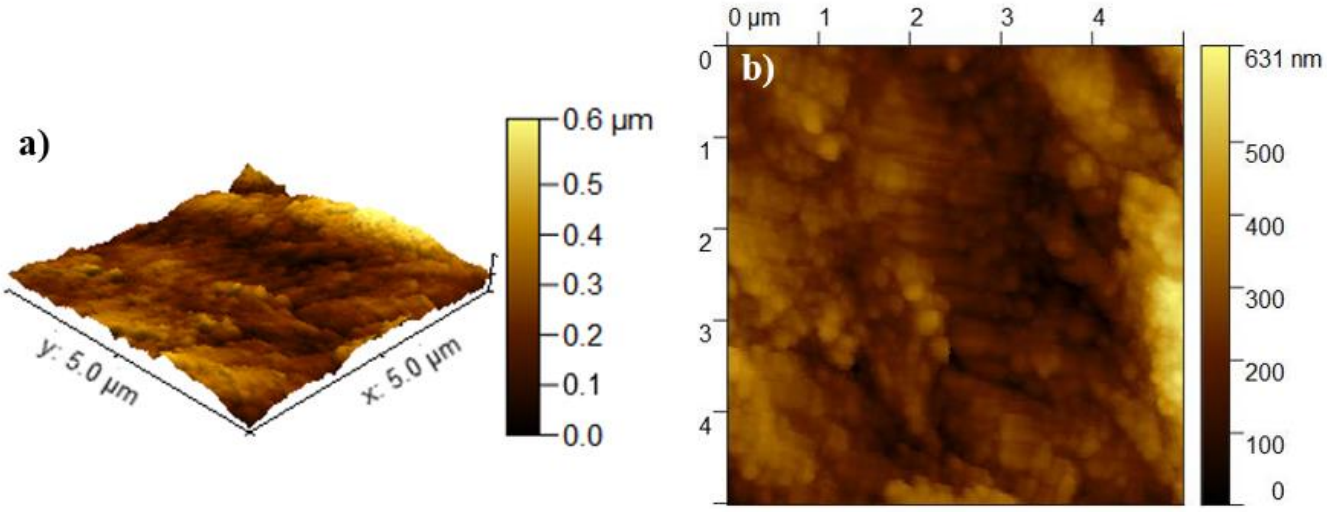

Figure 13- Gwyddion treated images of AFM topographical measurements on $FeCl_3$ -70°C for 5 minutes etched CC (a & b).

Figure 13 shows the topographical measurements of the chemical etched CC using $FeCl_3$-best conditions. It can be seen that the foil has improved roughness since the untreated metal foil is expected to be a very smooth surface, as some studies show for other metal foils [46]. Also, the AFM topographical image is coherent with the SEM results showing the uniform roughness validating that the etching took place along the entire surface. It seems that the roughness increased by the etched CC with $FeCl_3$, created a mountain-like and valley-like topography, with an overall higher surface irregularity. The surface roughness was evaluated by the root mean square (RMS) values. The obtained value for the $FeCl_3$ etchant solution was 88.14 nm. According to C2C, this value is within or higher than CCs showing satisfactory adhesion in previously tested experiments. Therefore, it is conclusive to say that the $FeCl_3$ solution based etched CC holds potential in improving the adhesion of the active material to the CC. However, the etched sample has marked irregularities in terms of mountains and valleys.

3.1.1.5 Characterization of dry-etched CCs

Dry etching was performed by plasma process bombarded with Ar and O_2 gases. It was done in two different ways: 1) Cleaned Ni foil was exposed to the Argon or O_2 plasma and 2) The Ni foil was first etched with the $H_2SO_4/H_2O_2/H_2O$ etchant solution and then exposed to Ar and O_2 gaseous plasma. The etchant solution used in this case was the best conditions of $H_2SO_4/H_2O_2/H_2O$. The mixed procedure of chemical and dry etching was experimented with the idea to further improve the chemically etched electrode after applying the gaseous plasma to the etched surface.

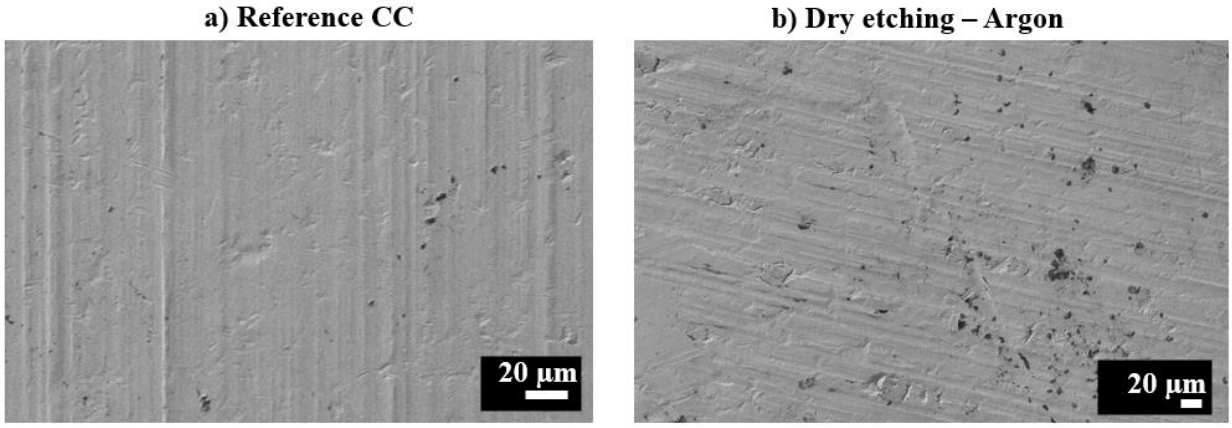

Figure 14- SEM images of a) Reference CC; b) dry etched CC using Argon.

The results are presented in **Figure 14**. The SEM image on etched CC (**Figure 14b**) demonstrates that there was no roughness observed on the surface after the plasma etching of the studied gases (Ar and O_2). To overcome this, more power and/or etching time could have been employed. Also, literature suggests other gases that can etch the surface but could not be employed in this work (Cl_2 and NH_3 [76]). The SEM image is relative to the Argon etching and it is possible to see that there is no apparent difference between the etched CC and the reference. However, through plasma etching, the adhesion can increase not only due to the roughness created[11]. This possible outcome was also analyzed through the electrochemical analysis.

The EDS analysis performed on the dry etching CCs also showed no residues of the etching procedure (annexes, **Figure 30, Figure 31, Figure 33, Figure 34**)

3.1.2 Screen-Printing

Some CCs were selectively etched by putting a mask on it through screen-printing. The idea behind this was to create a pattern in the Nickel foil. The mask used was provided by FCT-NOVA. The detail regarding the mask is presented in the annexes (**Figure 27**)

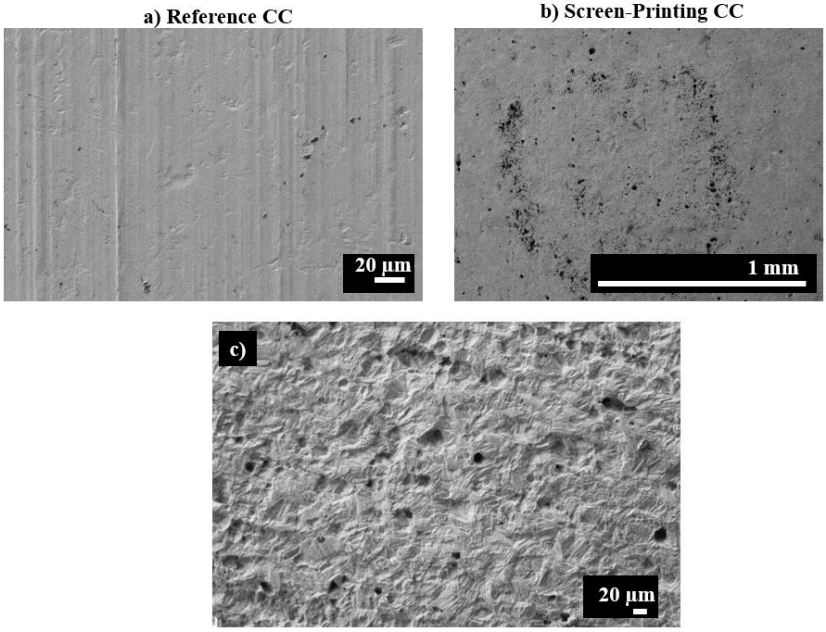

Figure 15- SEM images of a) Reference CC b & c) Screen-printed and etched CC using $FeCl_3$ etchant at different magnifications.

SEM was performed on the masked and the etched sample and is shown in **Figure 15**. Non-etched reference CC is also presented for comparison. The etching was performed under optimized conditions i.e., $FeCl_3$ at **70 °C for 5 minutes.** It is evident from the image (**Figure 15: c & d**) the formation of rougher surfaces in the unmasked region. It was also found that, even on putting two layers of masking, the acid penetrated through the resin and partially etched the undesired region. Also, through EDS analysis (**Figure 16**), it was possible to see the presence of titanium on the Ni foil surface. This means the mask containing the Ti particles, contaminated the Ni foil surface when treated with the acid, and these particles were not successfully removed with acetone. To conclude, screen-printing did not bring any significant advantages to the etching process.

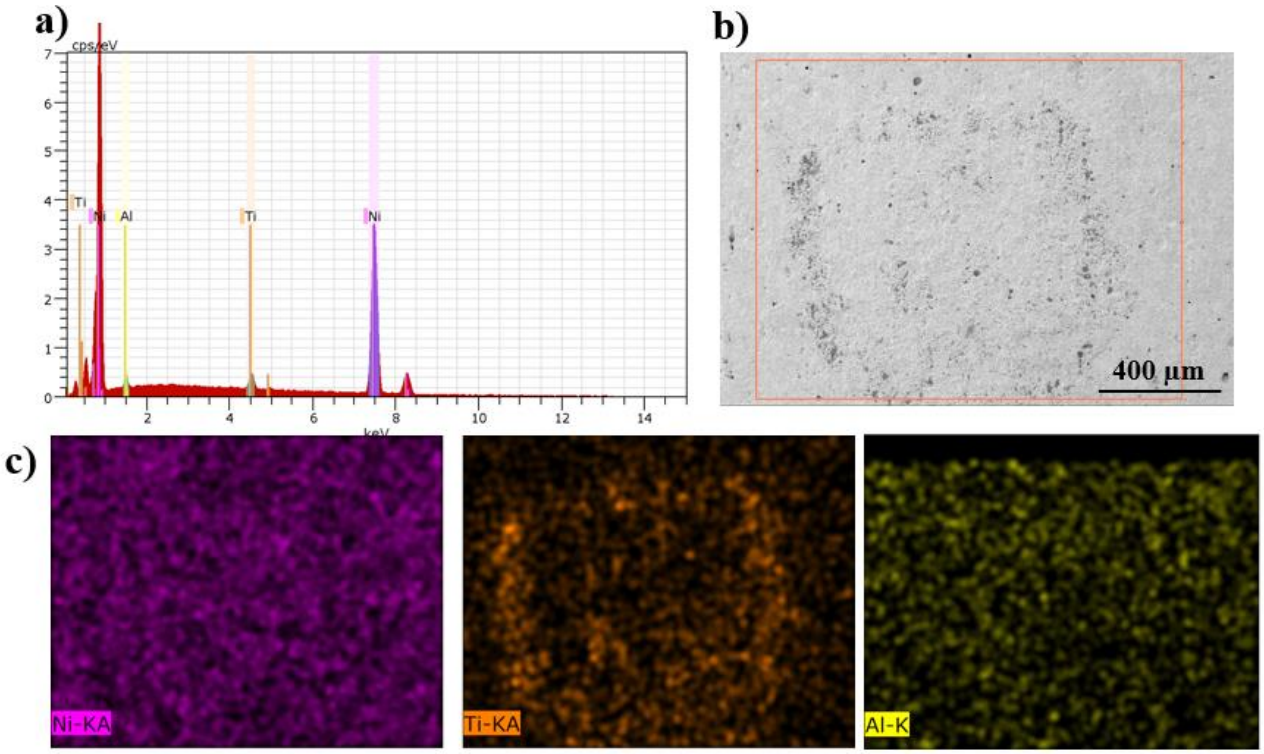

Figure 16- EDS test performed on the screen-printed CC. a) EDS spectrum, b) EDS layered image, c) EDS elemental mapping

3.1.3 Calendaring

Electrodes are generally calendared after coating the slurry to enhance its adhesion to the current collector and also to make electrodes uniform and smooth [11]. However, in this work, the calendaring approach was applied to generate the roughness to the Ni-foil surface using Ni-foam as a template. In that process, a thin Nickel foil (thickness 50 µm) was sandwiched between Ni foam as illustrated in **Figure 17.** Then, the foil was pressed by calendaring it. The visual image illustrated the roughness on the surface at macroscale. The roughness size was measured using *ImageJ* software and was found to be an average of 503 µm pore sizes (annexes, **Figure 29**). It is worth noting that this size is 100 times bigger than the carbon particle size. This mismatch

between the pores created by the calendaring and the carbon particle size can have a negative impact on the adhesion, as will be seen in the electrochemical analysis section.

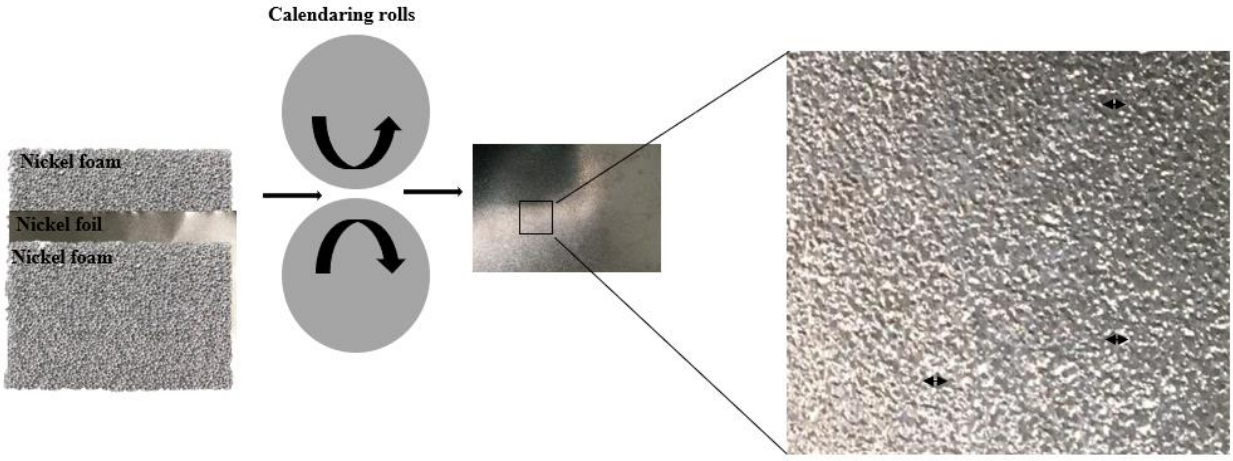

Figure 17- Schematic of the calendaring process employed to increase the roughness.

3.2 CONTACT ANGLE

The contact angle is a simple technique that is used in the study of surface engineering [77]. It provides information on the wettability of the current collector. Depending on the nature of the surface, the attractive force between the liquid molecules can be greater or smaller than the attractive force between the liquid molecule and surface interface, which determines the contact angle. The higher the surface energy, the larger the attraction of the liquid to the surface and higher the wettability, with a contact angle < 90°. On the contrary, the lower the surface energy, the drop of the liquid is repelled, and the contact angle goes higher than 90°. The ability to wet a surface is closely related to the adhesion characteristics of the surface, so the better the wettability (lower the contact angle) the better the adhesion [78]. These tests were done to evaluate the wettability of the treated electrodes in different etchant solutions. The contact angle measurement was done using DI water.

It can be observed from **Figure 18b** that the reference electrode has a completely hydrophobic behavior with a contact angle of 94°. In contrast, all the etched electrodes showed lower contact angles. The low contact angle was even more evident on the electrodes etched with $FeCl_3$ and $H_2SO_4/H_2O_2/H_2O$ etchant solutions. The contact angle using $FeCl_3$ etchant solution was determined to be 27˚. It was not possible to measure on the electrode etched with $H_2SO_4/H_2O_2/H_2O$ due to complete wetting, however, the contact angle was even lower than the one seen for the case with $FeCl_3$. Furthermore, on the screen-printed and etched electrode, the contact angle increased (**Figure 18e**) which might be due to the thin layer of unwashed resin on the surface, containing TiO_2 nanoparticles, that reportedly slightly increased the hydrophobicity and therefore the contact angle[79, 80]. The lower contact angle achieved after etching the Ni-foil is expected to improve the adhesion and further electrochemical performance.

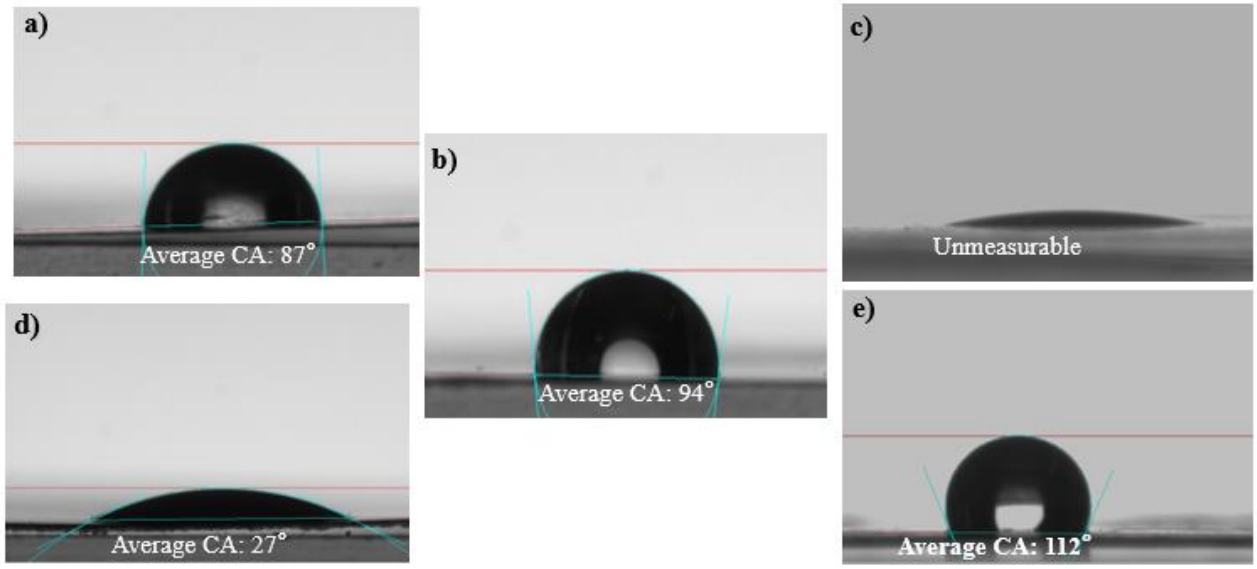

Figure 18- Contact angle measurements on CC after etching in: a) HCl/HNO_3 (best conditions); b) Reference; c) $H_2SO_4/H_2O_2/H_2O$ (best conditions); d) $FeCl_3$ (best conditions) and e) Screen printing and $FeCl_3$.

3.3 CROSS-CUT TEST

The cross-cut test is a very simple and effective method to assess the adhesion strength of the coated carbon slurry. This test can be done on the dry as well as wet electrodes which provides information on the degree of adhesion of active material to the CC [78].

The cross-cut test was performed on all the electrodes. Reference and benchmark electrodes were also analyzed and compared. The tests were repeated on three different electrodes in both dry and wet conditions to confirm the reproducibility of the result.

Two distinct observations were made when the test was done on the reference and benchmark electrode. When the cross-cut was made on dry electrodes the adhesion seemed to be satisfactory on both reference and benchmark electrodes, **Table 6 (**1a) and (1b). However, when the cross-cut test was done on the electrodes after 10 days immersed in the electrolyte (details for this procedure are provided in the materials and method section), the reference electrode showed a complete peeling of the coating as seen in **Table 6** (2a). In contrast, the benchmark electrode showed almost no flaking, meaning it has better adhesion and is the desired end product after following different etching techniques in the study.

Table 6- Cross cut tests performed on dry conditions and for 10 days in KOH with ISO classification for a) Reference CC and b) Benchmark CC

Sample	***1. Dry test***	***2. Test after10 days in KOH***	***ISO Classification for 10 days KOH***
a) Reference			5 (A degree of flaking that cannot be classified under any lower value)
b) Benchmark *Provided by C2C*		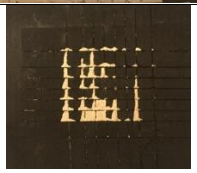	3 (The coating flaked along the edges of the cuts partly – represents more than 15% is affected but no more than 35%)

The cross-cut test results done on the electrodes made on chemically etched CC are presented in **Table 7**. The results reveal that the coating remains intact and showed good adhesion for all the electrodes in the dry

condition. However, the cross-cut test on the electrode where CC was etched in $FeCl_3$ solution showed improved adhesion even after putting the electrode in KOH solution for 10 days – see **Table 7** (2c). It is worth pointing that this result surpassed the adhesion strength of even the benchmark electrode as evidenced from the cross-cut results shown in **Table 6**(2b) and **Table 7**(2c). These improved results can be mainly attributed to the uniform roughness generated on the current collector after etching it in $FeCl_3$ (**Figure 12b**).

Table 7- Cross-cut tests performed on dry conditions and for 10 days in KOH with ISO classification for a)HCl/HNO_3 for 10 minutes; b)$H_2SO_4/H_2O_2/H_2O$ for 10 minutes and c)$FeCl_3$ for (70°C for 5 minutes)

Sample	***1. Dry test***	***2. Test after 10 days in KOH***	***ISO Classification for 10 days KOH***
a) *Best conditions – HCl/HNO_3* (10 minutes)		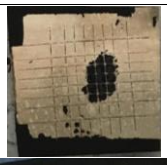	5
b) *Best conditions $H_2SO_4/H_2O_2/H_2O$* (10 minutes)		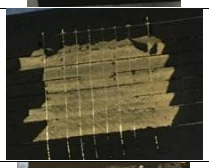	5
c) *Best conditions – $FeCl_3$* (70°C for 5 minutes)	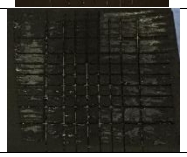		0 (None of the squares of the lattice is detached)

The cross-cut tests were also done on the electrode where the CC was dry etched. The results demonstrated in **Table 8** showed no peeling in the dry state, similarly as for the other electrodes tested but it completely peeled off when the electrode was subjected to the electrolyte for 10 days (**Table 8** (2)). The results can be related to the SEM images (**Figure 14**) where no roughness was observed on the surface after exposure to dry etching and that could be one possible reason for weak adhesion to the substrate.

Table 8- Cross-cut tests performed on dry conditions and for 10 days in KOH with ISO classification for a) Argon etching; b) Argon + etched ($H_2SO_4/H_2O_2/H_2O$ for 10 minutes) c) O_2 etching d) O_2 + etched ($H_2SO_4/H_2O_2/H_2O$) for 10 minutes

Sample	***1. Dry test***	***2. Test after 10 days in KOH***	***ISO Classification for 10 days KOH***
a) Argon			5
b) Etched foil ($H_2SO_4/H_2O_2/H_2O$ for 10 minutes) + Argon		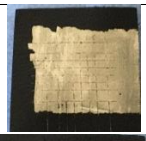	5
c) O_2			5
d) Etched foil ($H_2SO_4/H_2O_2/H_2O$ for 10 minutes) + O_2		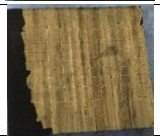	5

The cross-cut test on electrodes made on screen-printed and etched (using $FeCl_3$ etchant) CC (**Table 9**) also did not show any improvement in the adhesion of the coating.

Table 9- Cross-cut tests performed on dry conditions and for 10 days in KOH with ISO classification for a) Screen-printing and $FeCl_3$ etching for 70°C for 5 minutes

Sample	***1. Dry test***	***2. Test after 10 days in KOH***	***ISO Classification for 10 days KOH***
a) Screen Printing + $FeCl_3$ etching (70°C for 5 minutes)	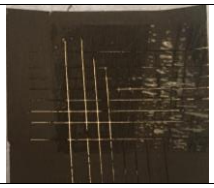	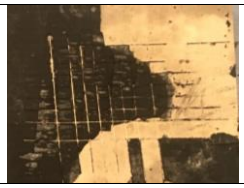	4/5

The electrode made on the calendared and etched CC (**Table 10**) also didn't show any improvement to adhesion as shown by the cross-cut test. This electrode has a similar peeling behavior as the reference.

Table 10- Cross-cut tests performed on dry conditions and for 10 days in KOH with ISO classification for a) Calendared not etched sample b) Calendared and etched ($FeCl_3$ etching for 70°C for 5 minutes).

Sample	***1. Dry test***	***2. Test after 10 days in KOH***	***ISO Classification for 10 days KOH***
a) Calendared not etched		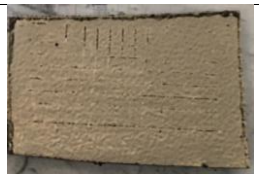	5
b) Calendared + etched ($FeCl_3$ at 70°C for 5 minutes) **The tests from both etching solutions ($FeCl_3$ and $H_2SO_4/H_2O_2/H_2O$) showed the same results. For this reason, only $FeCl_3$ is presented*	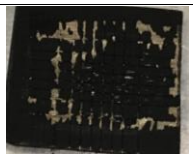		5

3.4 ELECTROCHEMICAL CHARACTERIZATION

The electrochemical characterization was carried out on all the etched samples. The tests were performed at ambient temperature (around 25°C). The dimensions of the electrodes were 7×7.5 cm^2. **Figure 19a)** demonstrates the arrangement of each component used for constructing electrochemical setup and **Figure 19b)** shows the 3-electrode setup used for the electrochemical measurements.

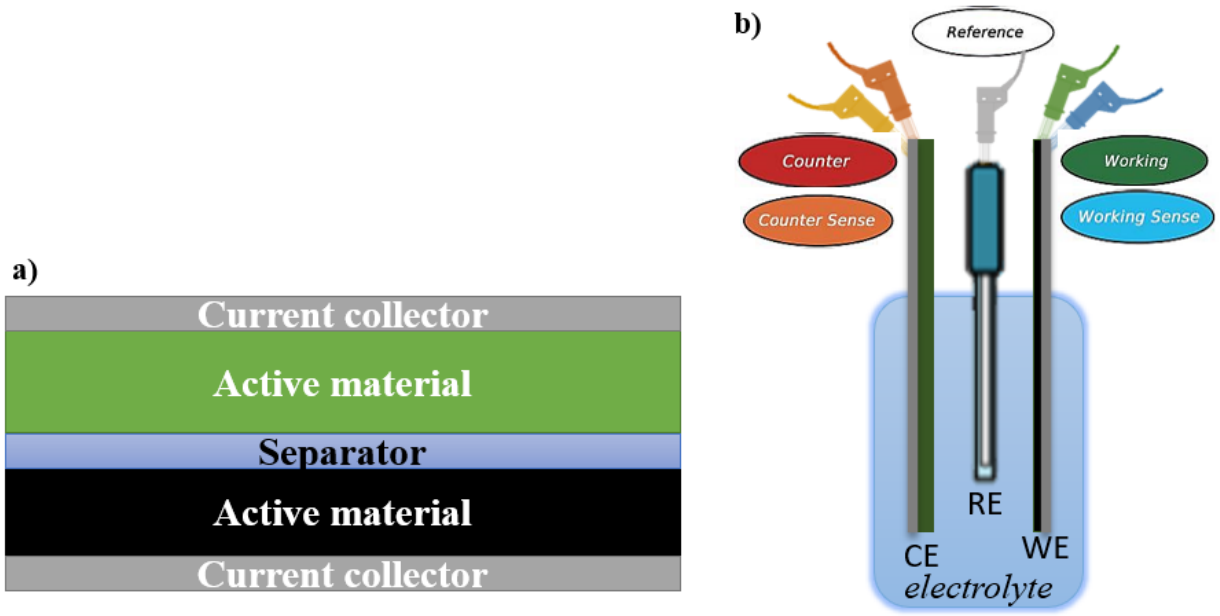

Figure 19- a) Schematic illustration of the cross section of cell setup; b) 3 electrode setup used for the electrochemical testing.

Electrodes were prepared on all the chemically and dry etched samples and characterized through electrochemical measurements by performing cyclic voltammetry (CV), galvanostatic charge-discharge (GCD), and electrochemical impedance spectroscopy (EIS) to understand the improved adhesion of the active material to the current collector. These measurements were also performed with the aim to identify the best etchant solution implemented throughout the work plan. Electrochemical measurements were also done on the reference and benchmark samples and compared.

In order to diminish the errors associated with the testing setup, reproducibility was tested. Within all the different etching employed, over 30 current collectors were tested. It was concluded that when testing a current collector from the same batch (same etching procedure and same coating procedure) under the same conditions (same setup, same electrolyte volume), there was an error in the ESR values obtained of ±0.008**Ω**. For the CV measurements at the same scan rate, the error was ±0.82V. This error can be due to the pressure applied, the amount of electrolyte used, as well as other factors related to the testing procedure. This has to be considered also when analyzing the results.

EIS measurements were done on the electrodes to interpret their resistive property. The hypothesis is based on the fact that increased roughness improves the adhesion and thereby lowers the interfacial resistance between the current collector and the active material.

EIS is composed of Nyquist and Bode plots. The Nyquist plot is the representation of the real *vs.* imaginary part of impedance as a function of frequency. **Figure 20** shows the obtained plot for an EDLC type electrode as well as the ideal plot for the same. Ideally, an EDLC has a nearly vertical line with a shift on the x-axis (due to the ESR) and the non-vertical component at intermediate frequencies originates due to ion transport limitations [81]. However, for some EDLC electrodes, the Nyquist is similar to **Figure 20**. In this plot, at high frequency (R_A) there is information on: (1) the bulk electrolyte resistance, (2) the resistance due to the ESR (the sum of resistance of the bulk electrolyte, connecting wires, and resistance originate from the type of CC used). Towards intermediate frequencies, the diameter of the semicircle (R_{AB}) has been attributed to (1) electrolyte resistance (in pores) (2) **contact resistance between electrode and current collector**, (3) charge transfer resistance. This charge transfer resistance in EDLC corresponds to the sum of the electrolyte resistance in the porous structure of the electrode, alongside with the electrode resistance, and the contact resistance between the electrode and the current collector.30 The mid-frequency region (R_{BC}) gives information on diffusion limited processes. A steep rise parallel to the imaginary axis at the low-frequency region indicates a capacitive behavior [12, 81, 82].

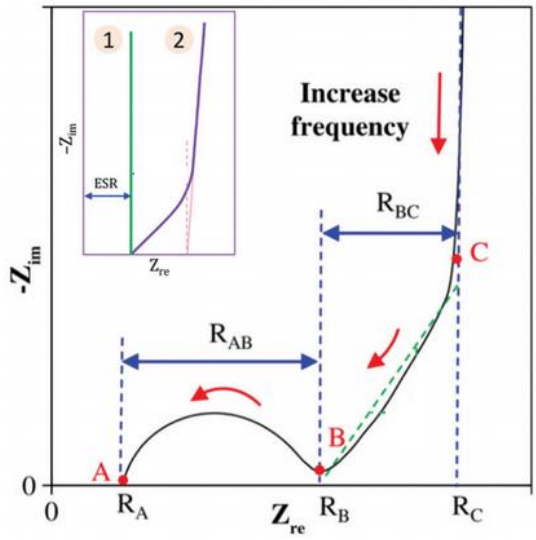

Figure 20- Schematic of typical Nyquist plots for an EDLC electrode. The inset shows a schematic representation of the Nyquist plot of an ideal capacitor (line 1) and electrochemical capacitor with porous electrodes (line 2). Retrieved from [81].

EIS measurement was done on all the electrodes made after etching the current collector. The Nyquist part of the EIS performed at OCP is presented in **Figure 21**. **Figure 21a)** presents the Nyquist result of electrode made on CC etched using $H_2SO_4/H_2O_2/H_2O$ solution for different times. The results from the high-frequency response clearly evidenced the low resistance for the electrode etched for 10 minutes. Furthermore, the electrode etched for 10 minutes also showed an improved current response in CV measurement when compared to other electrodes at 30 mV s^{-1}(Annexes, **Figure 35b**) and the higher phase angle in the bode plot (Annexes, **Figure 35b**). The impedance results on electrodes made after etching the CC in $FeCl_3$ for 2, 5, and 10 minutes at 40 and 70 ˚C are presented in **Figure 21b)**. The CC when etched for 5 min at 70 ˚C showed comparatively lower ohmic resistance, around 0.004Ω lower than the second-best solution (10 minutes at 40°C). Nevertheless, and considering that there is not a correlation for the best solution (more time does not induce the best etching as well as more temperature) the errors previously explained related to the testing setup can influence these results since between the best solution and the worst there is a 0.008Ω difference, which corresponds to the error in the setup. It is also evident from the magnified view of the Nyquist plot that the resistance of the best electrode made after etching in $FeCl_3$ has almost one order of magnitude lower resistance than the electrode made after etching in $H_2SO_4/H_2O_2/H_2O$ solution. The impedance results in the low-frequency region showed more inclination towards the imaginary axis which was also reflected in the bode plot possessing a high phase angle around -90˚ showing very good capacitive property (Annexes, **Figure 35d**). The results on electrodes made after etching CC in HCl/HNO_3 solution for 3, 5, and 10 minutes are given in **Figure 21c**). The results showed that the contact resistance for the electrode etched for 3 minutes is slightly lower (seen by the intersection of the plot with the x-axis) however the ohmic resistance, which mainly comes from CC and the active material interface is much lower for the electrode made after etching CC for 10 minutes (semicircle). This was further confirmed by CV measurements that showed a higher current response for the 10-minute electrode (Annexes, **Figure 35a**). Though the results for the 10 minutes in this etching solution demonstrated an improvement by a decrease in the interfacial resistance, it is still higher when compared to the results obtained in $FeCl_3$ case (**Figure 21b**)). The EIS results on electrodes made after physical and chemical + physical etching of CC are presented in **Figure 21d**). There is no significant improvement observed in the results obtained on the electrodes after etching only through Ar bombardment and after the chemical etching + Ar bombardment. Also, the resistance obtained for the electrodes in both cases are higher than the electrodes made after etching CC in $FeCl_3$ solution- refer to **Figure 21(b & d)**.

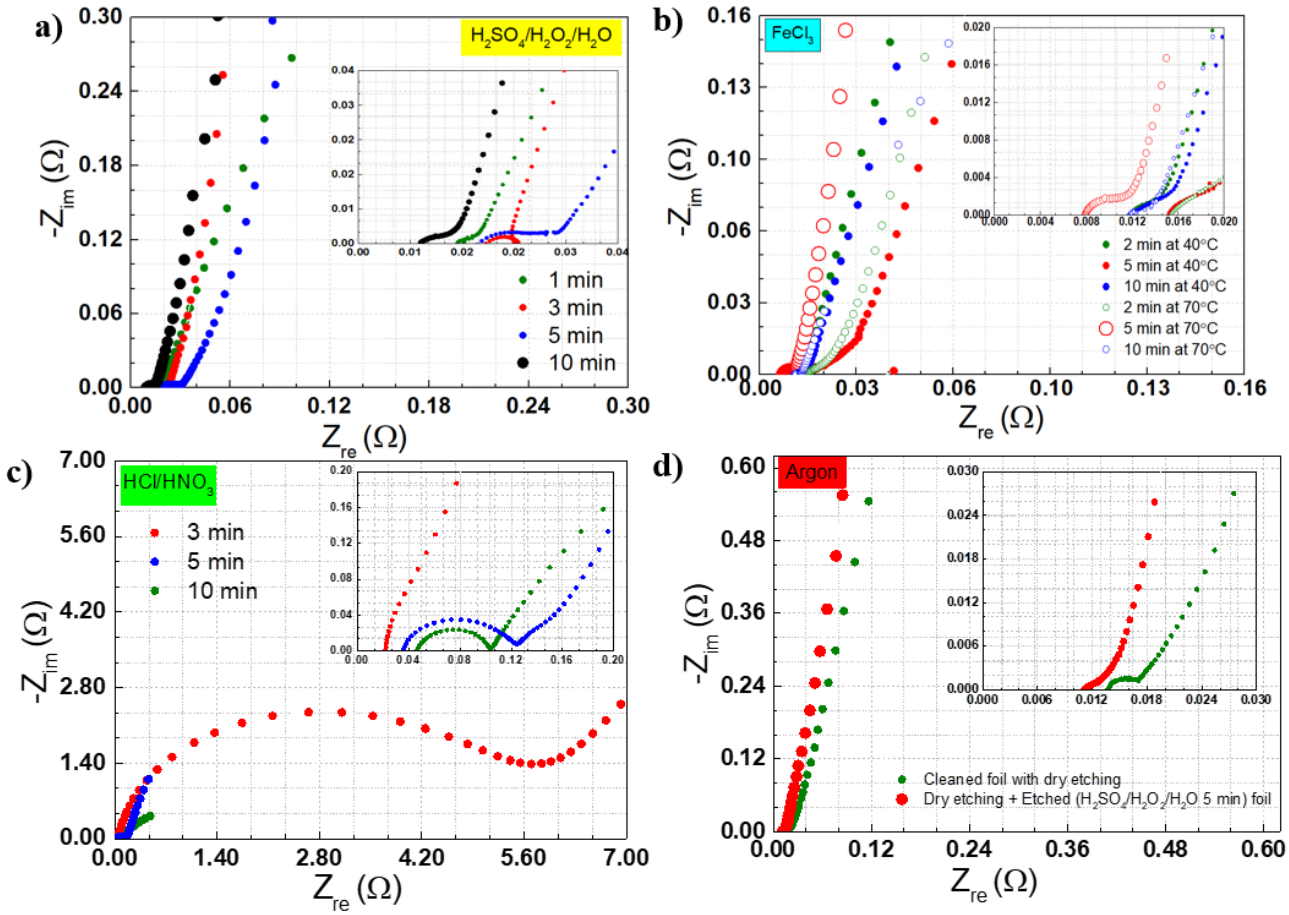

Figure 21- Nyquist plots on a) $H_2SO_4/H_2O_2/H_2O$ etchant solution at different times; b) $FeCl_3$ etchant solution at different times and temperatures; c) HCl/HNO_3 etchant solution on different times and d) Argon etching with and without chemical etching.

Table 11 summarizes the best etching parameters obtained from the EIS and CV results, based on the conclusive remarks described above.

Table 11- Best conditions obtained for each etching solution.

Etching Solution	***Best conditions***
$H_2SO_4/H_2O_2/H_2O$	10 minutes
$FeCl_3$	5 minutes at 70°C
HCl/HNO_3	10 minutes
Dry etching	Etched ($H_2SO_4/H_2O_2/H_2O$) + Ar

Figure 22a&b shows the results for the calendared CCs and etched ($FeCl_3$ and $H_2SO_4/H_2O_2/H_2O$). The EIS analysis shows that a smaller gap in the calendar shows better results, with both etchant solutions. However, the electrochemical results did not improve much when compared to the electrode made on directly etched CCs. This implies that the calendaring process did not bring any significant difference in the electrochemical results.

Selective etching was done on the CC after screen-printing on it in the chosen pattern, composed of small circles where the resin would be fixated. The etching was done using $FeCl_3$ solution. The EIS measurements done on the electrode prepared on treated CC are given in **Figure 22c**. It is found from the Nyquist and Bode results (annexes, **Figure 36**) that there was not an improvement in the interfacial resistance (ESR) after screen printing followed by etching the CC compared to $FeCl_3$ etching treatment. Therefore, it can be said that the screen-printing + etching process was not an effective approach and didn't improve the adhesion of active material to the CC.

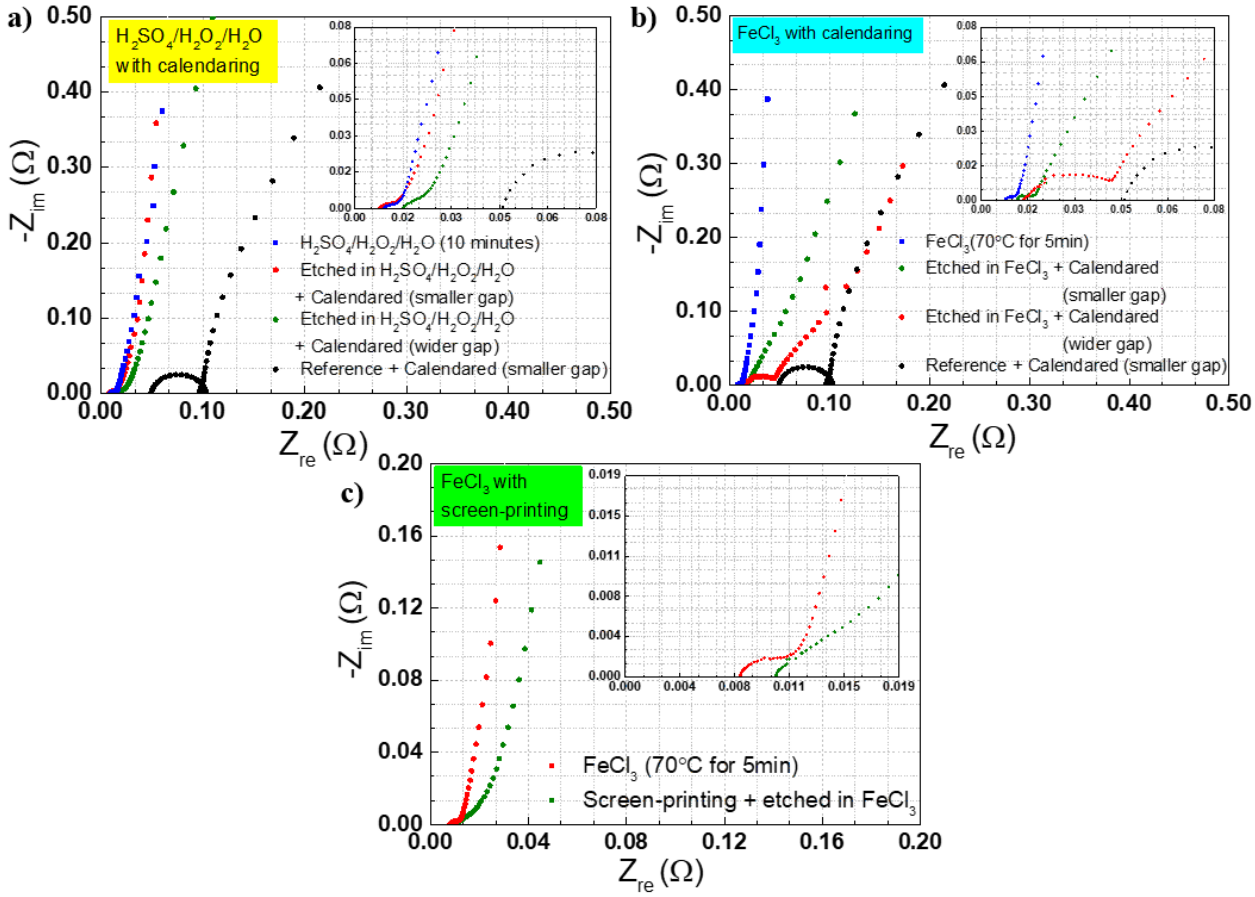

Figure 22- Nyquist plots for a & b) Calendaring process with previous etching from $H_2SO_4/H_2O_2/H_2O$ and $FeCl_3$ etchant solutions. In c) Screen-printing process followed by etching in $FeCl_3$ etchant solution.

The EIS performance of all the electrodes prepared after etching the CC under the best conditions are compared in **Figure 23a)**. It is clearly evident from the high-frequency results of the Nyquist plot that all the electrodes made on etching the CC in different etchant solutions have lower ESR meaning better performance compared to the electrode made on Ni-foil without any etching denoted in the plot as "reference". Among the electrodes prepared on etched CC, $FeCl_3$ etchant solution seems to be the most promising as the electrochemical test on the electrode made on $FeCl_3$ etched CC evidenced the lowest ESR. The good result obtained in the $FeCl_3$ case could be possibly due to the improved adhesion which was clearly observed from the cross-cut test (**Table 7c**). This improvement could be attributed to the homogenous roughness generated on the surface after etching as evidenced from SEM and AFM images (**Figure 12** and **Figure 13**) and also to the significant improvement in the hydrophilicity of the surface after the etching where the contact angle measurement evidenced a sharp lowering in the angle: 94˚ in reference vs. 27˚ after $FeCl_3$ etching **(Figure 18**).

The electrochemical results on benchmark and $FeCl_3$ etched CC electrodes are compared and presented in **Figure 23(b-d)**. The Nyquist plot along with the bode plot indicated slightly better results for the $FeCl_3$-best conditions, with a lower ESR (**Figure 23b&c)**) and a higher phase angle (**Figure 23d)**), indicating also a more capacitive behavior. These results were coherent with the physical characterization (SEM and AFM), which showed that the $FeCl_3$ had a surface more inclined to improve the adhesion and therefore improve the electrochemical performance.

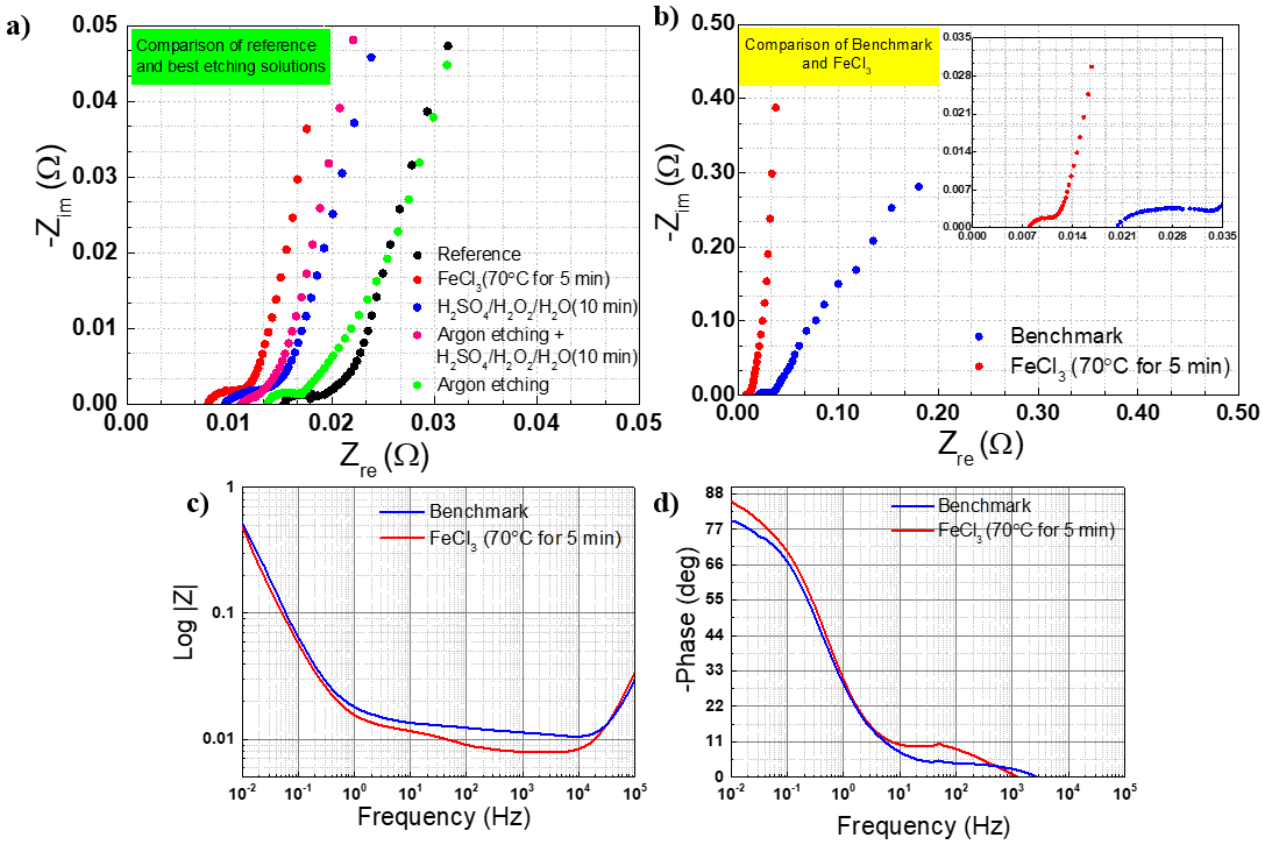

Figure 23- Comparison plots of a) the best conditions obtained for each etching solution and the reference electrode; b-d), present the electrochemical impedance spectroscopy for the best conditions among all the etching solutions ($FeCl_3$ at 70°C for 5min) and the benchmark electrode.

EIS data obtained from the measurements done on the electrodes made after etching the CC in the best etching solution i.e. $FeCl_3$ at 70 ˚C for 5 min and reference were fitted using a suitable equivalent circuit. The equivalent circuit was used to interpret the EIS data and quantify the ESR values. The equivalent circuit used in this work is very similar to a Randles circuit. It is composed of R_1, representing the ESR, followed by a constant phase element (CPE), representing the double layer capacitance, and in parallel, a resistor R_2 that is attributed to the charge transfer resistance in series with an infinite Warburg element, a specific electrochemical element of diffusion. The fitting was done using the *Gamry Echem Analyst* software properties [83, 84].

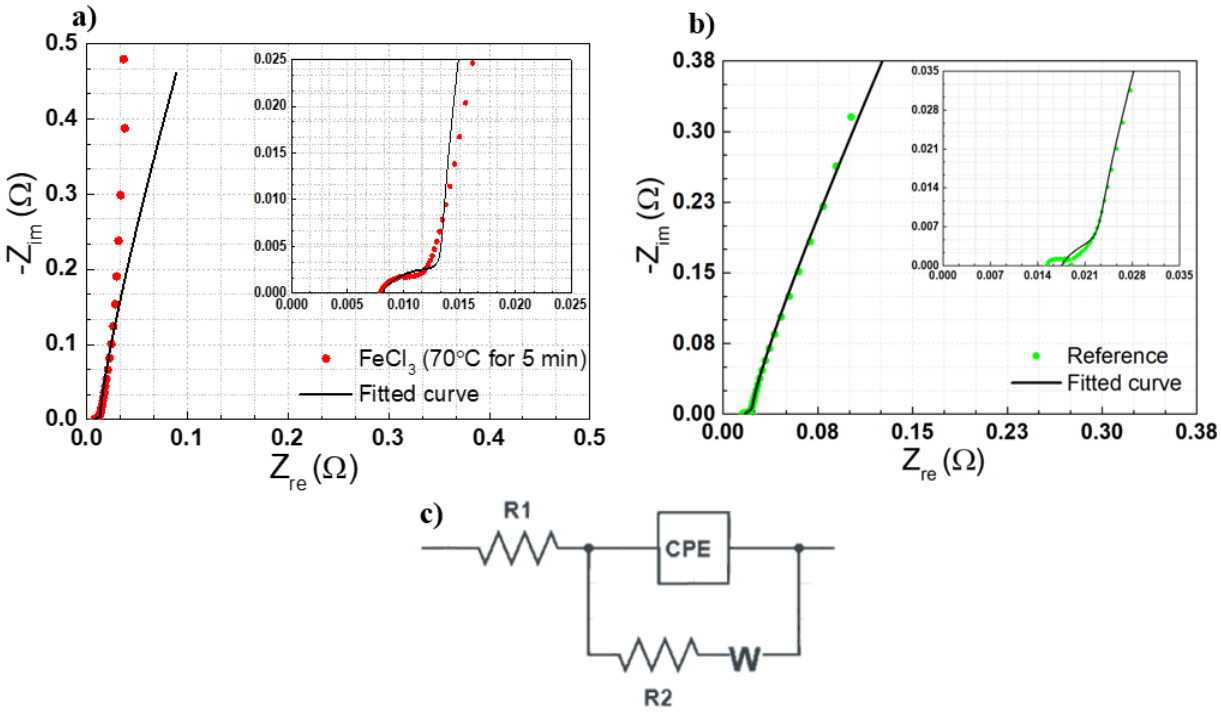

Figure 24- Results for the fitted curves are presented for a) the best etching solutions: b) the reference electrode. c) equivalent circuit model used for the fittings.

The fitted results along with raw data for the $FeCl_3$-best condition and the reference electrodes are presented in **Figure 24a)** and **b)**. The ESR value which is attributed to R_1 in the circuit was obtained to be **0.008 Ω for the $FeCl_3$**, and **0.021 Ω for the benchmark** electrode. These results further strengthen $FeCl_3$ as a better etchant solution resulting in lower ESR mainly originating from the increased adhesion.

To further evaluate the adhesion strength, the electrode on $FeCl_3$ etched CC, benchmark and reference were subjected to aggressive electrochemical testing and the performance was compared. To test the adhesion in the aggressive condition, the electrodes were conditioned at -1.2 V which is beyond the stability zone for the carbon-based materials, and kept for 30 minutes. Further CV and EIS were performed on the electrodes before and after this test in a stable potential window of -1 to 0 V at 30 mV/s to monitor the changes in the performance and the respective results are presented in **Figure 25**. From that, it could be concluded that the sample with the lowest decrease in peak current would be the best, at the same scan rate. The benchmark has the lowest decrease in peak current after the aggressive test, contrasting with the reference electrode, whose pronounced decrease is visible. The $FeCl_3$ also shows a decrease in the peak current, even though it is not as pronounced as the reference. The response curve does not have a rectangular shape, indicating an increase in the ESR after the aggressive test. The reason for this decrease could be ascribed to the peeling of the coating due to the stress imposed on the sample with the aggressive test. As such, in this studied parameter the benchmark sample had better performance. This was also cross-checked with the impedance results that were performed before and after the aggressive test. These results are in annexes **Figure 38**. For the reference electrode, it was not possible to present the results due to the complete peeling of the coating. The plot shows that, in comparison with the benchmark, the $FeCl_3$ performance decreased a lot after the aggressive test, with a much higher ESR than the benchmark and the same sample at OCP. This is therefore coherent with the CV analysis.

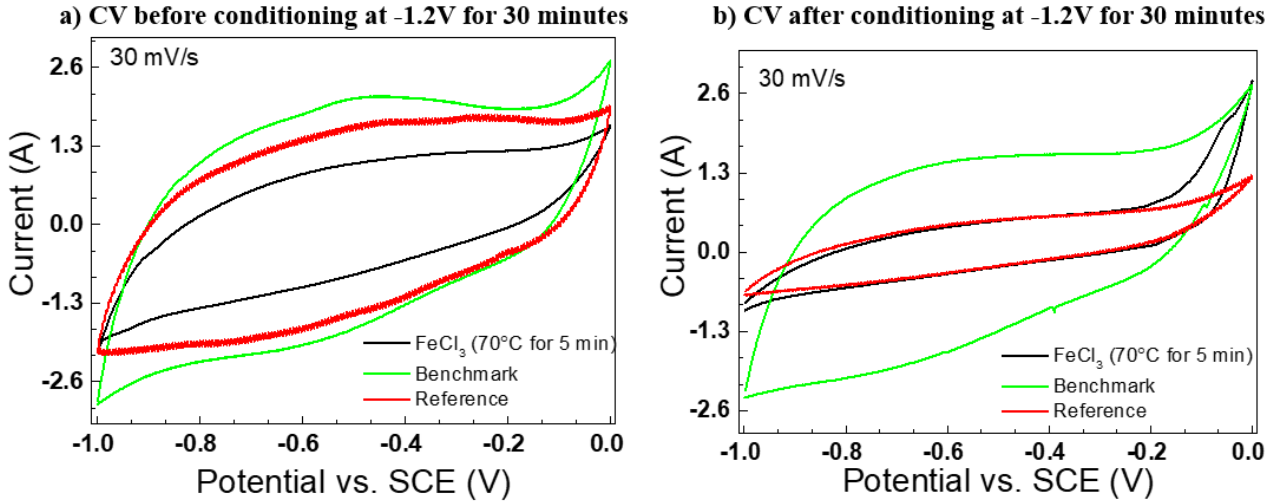

Figure 25- CV for a) $FeCl_3$, benchmark and reference electrode at 30 mV/s before conditioning at -1.2V or 30 minutes and b) $FeCl_3$, benchmark and reference at 30 mV/s after conditioning at -1.2V for 30 minutes.

Cyclic testing was further done on both electrodes- Reference, and $FeCl_3$ etched CC (**Figure 26**). The electrodes were cycled in a three-electrode setup up to 2000 cycles at 1 A. The parameters such as the evolution of capacitance, coulombic efficiency, and stability with cycling were monitored. The capacitance was calculated from the discharge curve using $C = I \times \frac{\Delta T}{\Delta V}$(Equation *1*Equation 1.

$$C = I \times \frac{\Delta T}{\Delta V} \text{(Equation 1)}$$

Where I is the constant discharging current (A), ΔT is the discharge time (s), and ΔV the potential window (V).

The coulombic efficiency was calculated using the ratio of charge and discharge time according to $\eta = \frac{t_D}{t_C} \times 100\%$ (Equation *2*Equation 2. ([85, 86]):

$$\eta = \frac{t_D}{t_C} \times 100\% \text{ (Equation 2)}$$

Where t_D and t_C refer to discharge and charge time, respectively.

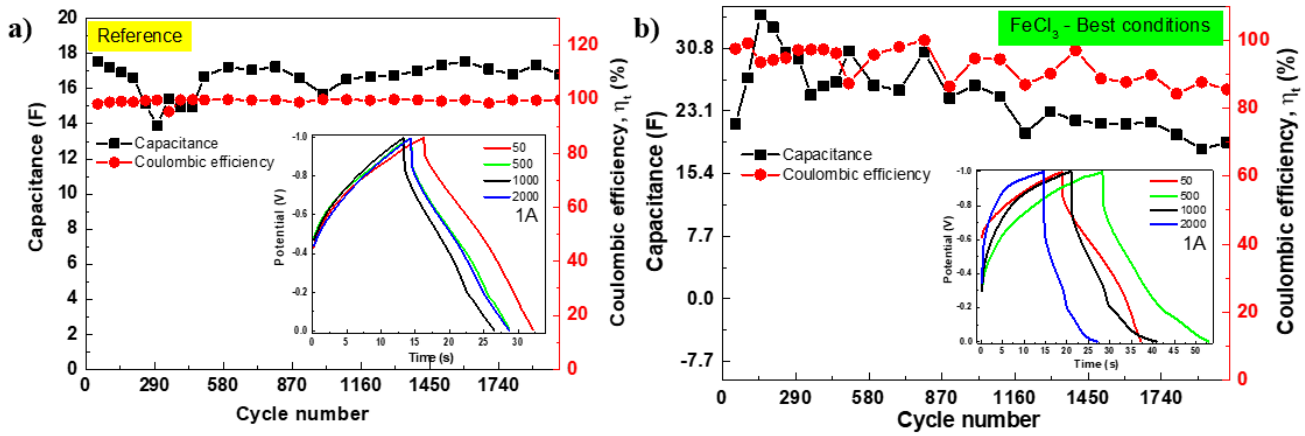

Figure 26- Capacitance and coulombic efficiency for a) the reference CC ; b) the $FeCl_3$ electrode up to 2000 cycles. Inset showing the charge-discharge profile after a certain number of cycles.

The average capacitance obtained for the reference was **16.5 F,** and **25.3 F** for the electrode on $FeCl_3$ etched CC. The electrode made on $FeCl_3$ etched CC presented higher capacitance compared to the reference,

in one way indicating the improved adhesion of the material to the current collector. This electrode also showed better results compared to the electrodes made on CC etched with other etching solutions (shown in Annexes, **Figure 39**). However, its stability was not as good as desired, since it dropped from 34 F in the first cycles to 19F after 2000 cycles. Furthermore, the CD plots in the inset of the graphs show an IR drop for all the tested samples, indicating higher resistive property than desired. This is visible in the $FeCl_3$ etchant solution, which was not expected. This drop was similar among all the tested samples and increased with the increase in cycles [85]. Therefore, the electrode stability upon etching should be further studied and improved.

The main results obtained for the above graphs are summarized in **Table 12**.

Table 12 - Results obtained for the best etching solution and the reference and benchmark

Etching Solution	***ESR(Ω)***	***Average Capacitance(F)***	***Average Coulombic efficiency (%)***
Reference	0.021	16.5	99.5
$FeCl_3$- Best conditions	0.008	25.3	92.8

With this conclusion, which shows that the best etching solution was the $FeCl_3$ etchant at 15%, a simple estimation on the implementation price for scaling-up can be done. This estimation considers the quantity of solution that is used per sample, with which frequency the etching solution has to be replaced, and the price per kilo of the etchant solution at a purity of at least 98%. With this, this work enabled to conclude that the estimated price of the etching solution alone was 23€/m^2 of the metal foil.

Despite this representing a significant price increase, strategies to overcome this could be further studied and employed. During the course of this work, there was already a successful attempt to reduce the concentration of the etchant solution and increase the temperature, achieving satisfactory results. This was achieved by reducing the concentration from 30% to 15%. Therefore, reducing further from 15% to 7.5 % may lead to similar results if time and temperature are adjusted.

Also, recycling techniques have been reported and could be adopted in this case to tackle the cost problem, as well as reducing the polluting residues[87]. Recycling techniques that can recover the waste solution, as well as the metal, consist of iron powder replacement method, ionic electrolysis membrane method, and crystallization method, among others. However, these processes are very complex to implement into a manufacturing line and have some disadvantages associated. Literature highlights the crystallization method as a very advantageous one, since it does not introduce additional substances, has a low operating temperature, can improve the operating environment, and can accomodate modifications in order to ease the scale-up process. According to X. F. Miao et al, this upgrade would be able to recover up to 56% of the etchant solution using the process described in literature. Such an upgrade and development would therefore hold the potential to even reduce the cost to 10€/m^2 per recycling cycle.

4 CONCLUSIONS AND FUTURE PERSPECTIVES

The main goal of this master's thesis work was to develop a surface treatment technique on the nickel foil to increase the adhesion of the carbon coating on the current collector (CC) to obtain low interfacial resistance as well as to improve the long-term stability of asymmetric supercapacitor. This study focused on generating roughness on the CC employing many etching techniques.

The etching effects were studied by varying both etching time and temperature. The Physico-chemical characterizations were performed on etched CC following SEM and AFM to analyze the roughness created on the CC. Further, electrodes were made on all etched CC and cross-cut tests were done to check the adhesion of the coating. Electrochemical measurements were made by performing EIS and CV to evaluate the changes in the performance after CC surface treatment. This test also guided in finding the optimum parameter for each etching procedure. The results were also compared to the benchmark i.e., electrodes with satisfactory adhesion provided by C2C for comparison of results, and reference i.e.,carbon coated on CC with smooth surface and without any prior treatment. Among the chemical etching solutions tried, the best result was obtained for a 15% concentration of $FeCl_3$ at 70°C for 5 minutes. SEM and AFM evidenced a homogenous roughness created on the surface which possibly helped in improving the adhesion as evidenced from the cross-cut tests. EIS results further showed a significant improvement in the performance compared to the reference electrode where ESR values lowered (0.008Ω in $FeCl_3$ etched electrode *vs.* 0.021 Ω for reference electrode). The results after etching the CC in $FeCl_3$ also showed even better results to the reference electrode in terms of capacitance (51% increase) even though the coulombic efficiency performance had not improved. This evidenced the positive impact of the etching process prior to coating the carbon on it.

Other than chemical etching, screen printing was implemented to create a pattern that could mimic the size of carbon particles and thus create better anchor points between the Ni-foil and the carbon material. This idea was applied to improve the performance further than what was obtained after only etching in $FeCl_3$. However, the etching solution penetrated into the resin and thereby the results did not show any improvement on the performance. The screen-printing etching process carries a room of improvement where a hydrophobic inert polymeric layer can be patterned over the thick resin mask to inhibit the solution from penetrating throughout. Other than screen printing, plasma etching was also experimented mainly because it holds the possibility of scaling up the process. However, the results obtained from physical characterization on CC, cross-cut tests and electrochemical results on the electrodes were not satisfactory.

In conclusion, the best result in terms of adhesion, cross-cut tests and electrochemical measurements obtained was from chemical etching using 15% $FeCl_3$ at 70°C for 5 minutes. This thesis thus allowed for a fitting solution to enhance the adhesion between the current collector and the active material for a better supercapacitor performance. The results also enabled the correlation between the etching with the wettability of the electrodes and its adhesion. Through this study, different information was compiled regarding the different techniques available, their outputs, advantages, and disadvantages, backed up by the electrochemical analysis and the physical characterization. Also, even though there is a scale-up ability for this solution, this should be improved, taking in consideration that the price is not competitive with the solutions employed by C2C. Regarding this etchant solution, process issues can be a limiting factor (such as the need to always keep the solution under high temperature for the etching). Safety may constitue a problem, even though this solution was the safer among the chemical etchants.

Table 13 details the main conclusions above enlightened that were attained by electrochemical characterization.

Table 13- Main conclusions inferred from electrochemical analysis following the procedure detailed in Chapter 2

Testing procedure	***Parameters obtained***	***Main conclusions***
1) Electrochemical impedance spectroscopy (EIS)	Nyquist plot (from which value of ESR was retrieved), bode plot	Best chemical etched sample ($FeCl_3$-best conditions) performed better than the reference electrode (ESR 2.6 times smaller)
2) Cyclic voltammetry (CV)	Peak current, capacitive behaviour	Best performance for $FeCl_3$-best conditions. All etched samples performed better than the reference electrode.
4) EIS after aggressive test (30 minutes at -1.2V)	Same as for 1	Decrease in performance in all the tested samples, that suggests a peeling of the coating.
5) CV after aggressive test (30 minutes at -1.2V)	Same as for 2	Same outputs as for 4).
8) Charge-Discharge (CD)	Capacitance, coulombic efficiency, cycle stability	$H_2SO_4/H_2O_2/H_2O$ had higher Capacitance, followed by $FeCl_3$ by a difference of 0.1F. $FeCl_3$ did not show the best coulombic efficiency, but overall performance was satisfactory. Lowest capacitances decrease in reference and HCl/HNO_3-best conditions samples (that also had lowest capacitances).

4.1 FUTURE PERSPECTIVES

Regarding the future prospects of this subject, all the processes employed could be further optimized and improved. More chemical etching solutions [51], electrochemical etching or different gases in the dry etching [87] could be further studied. To complement this study, different patterning techniques have also been reported on different substrates and could be studied further, such as laser patterning, inkjet-printing and others that could allow for the creation of microholes that would anchor the active material particles [61, 88, 89, 90].

Ni foil is a very attractive material as a current collector for supercapacitors due to its low price compared to other substrates and its inertness. Therefore, other methods to create roughness, thus enhancing the performance, are also being studied and have an optimistic future, such as physical exfoliation, a straightforward method using only a stamp to peel the material and without the need for a special apparatus [91]. Other approaches to enhance the adhesion is also an emerging field. In the course of this work, it was intended to study the UV treatment in the Ni foil and to analyse its effect on wettability and adhesion but due to the COVID-19 lockdown this was not possible to do. Therefore, this would be of interest in future studies.

Within this framework, many other factors related to the adhesion can be studied and correlated, other than the roughness of the foil (leading to a higher surface area), such as surface tension and wettability. Treatments such as corona discharge can be used to improve the wettability and the surface tension. This treatment is based on high-frequency discharges, that already showed promising results in terms of both performance and scale-up ability [11, 92]. In this treatment, the substrate to be etched is bombarded with high-speed electrons that cause the substrate modification [93]. This is very advantageous compared to plasma etching since it can treat substrates of any size and shape.

Other factors that can impact the adhesion can be related to the binder amount in the active material and the coating thickness of the same. Both these factors can also be studied and optimized.

Additionally, turning the plane foil surface into a porous one has been reported as a captivating perspective. This can be achieved through the construction of nanowires on the surface by different methods, such as self-assembly [94].

Finally, it is of interest in future studies to find new and inventive ways to enhance the adhesion using the above-described methods at an industrial level. This step is very important towards the production of supercapacitors with the performance proven in literature at a large scale. To this end, the lab scale processes need to be studied and scaled-up.

5 BIBLIOGRAPHY

[1] E. Hossain, H. M. R. Faruque, M. S. H. Sunny, N. Mohammad, and N. Nawar, "A comprehensive review on energy storage systems: Types, comparison, current scenario, applications, barriers, and potential solutions, policies, and future prospects," *Energies*, vol. 13, no. 14, pp. 1–127, 2020, doi: 10.3390/en13143651.

[2] "Electricity map." https://www.electricitymap.org/zone/IS (accessed Feb. 16, 2021).

[3] "Gail Tverberg: An Energy/GDP Forecast to 2050." https://peakoil.com/consumption/gail-tverberg-an-energygdp-forecast-to-2050 (accessed Feb. 19, 2020).

[4] "Renewable capacity additions by country/region 2019-2021." https://www.iea.org/data-and-statistics/charts/renewable-capacity-additions-by-country-region-2019-2021 (accessed Dec. 10, 2020).

[5] "Supercapacitors Market - Growth, Trends, COVID-19 Impact, and Forecasts (2021 - 2026)." https://www.mordorintelligence.com/industry-reports/supercapacitors-market (accessed Feb. 18, 2020).

[6] E. technology and innovation Platform, "Strategic Research Agenda for batteries 2020," 2020. [Online]. Available: https://ec.europa.eu/energy/topics/technology-and-innovation/batteries-europe/news-articles-and-publications/sra_en.

[7] A. Afif, S. M. Rahman, A. Tasfiah Azad, J. Zaini, M. A. Islan, and A. K. Azad, "Advanced materials and technologies for hybrid supercapacitors for energy storage – A review," *J. Energy Storage*, vol. 25, no. July, p. 100852, 2019, doi: 10.1016/j.est.2019.100852.

[8] O. Balch, "The curse of 'white oil': electric vehicles' dirty secret," 2020. https://www.theguardian.com/news/2020/dec/08/the-curse-of-white-oil-electric-vehicles-dirty-secret-lithium?fbclid=IwAR3UdK84D9nkPZXmxkz5oif8xaIKePhqJQ7f5NzHmfsbA-Fsdt1TjjVuevo (accessed Oct. 12, 2020).

[9] S. Huang, X. Zhu, S. Sarkar, and Y. Zhao, "Challenges and opportunities for supercapacitors," *APL Mater.*, vol. 7, no. 10, 2019, doi: 10.1063/1.5116146.

[10] Martha Ekkert, *Global energy transformation: a roadmap to 2050*. 2018.

[11] N. Billot *et al.*, "Investigation of the Adhesion Strength along the Electrode Manufacturing Process for Improved Lithium-Ion Anodes," *Energy Technol.*, vol. 8, no. 2, 2020, doi: 10.1002/ente.201801136.

[12] A. Noori, M. F. El-Kady, M. S. Rahmanifar, R. B. Kaner, and M. F. Mousavi, "Towards establishing standard performance metrics for batteries, supercapacitors and beyond," *Chem. Soc. Rev.*, vol. 48, no. 5, pp. 1272–1341, 2019, doi: 10.1039/c8cs00581h.

[13] X. Luo, J. Wang, M. Dooner, and J. Clarke, "Overview of current development in electrical energy storage technologies and the application potential in power system operation," *Appl. Energy*, vol. 137, pp. 511–536, 2015, doi: 10.1016/j.apenergy.2014.09.081.

[14] H. Chen, T. N. Cong, W. Yang, C. Tan, Y. Li, and Y. Ding, "Progress in electrical energy storage system: A critical review," *Prog. Nat. Sci.*, vol. 19, no. 3, pp. 291–312, 2009, doi: 10.1016/j.pnsc.2008.07.014.

[15] J. Liu *et al.*, "Advanced Energy Storage Devices: Basic Principles, Analytical Methods, and Rational Materials Design," *Adv. Sci.*, vol. 5, no. 1, 2018, doi: 10.1002/advs.201700322.

[16] B. E. Conway and B. E. Conway, "Similarities and Differences between Supercapacitors and Batteries for Storing Electrical Energy," *Electrochem. Supercapacitors*, no. 2, pp. 11–31, 1999, doi: 10.1007/978-1-4757-3058-6_2.

[17] V. S. BAGOTSKY, A. M. SKUNDIN, and Y. M. VOLFKOVICH, *ELECTROCHEMICAL POWER SOURCES- Batteries, Fuel Cells, and Supercapacitors*. 2015.

[18] B. Dunn, H. Kamath, and J. M. Tarascon, "Electrical energy storage for the grid: A battery of choices," *Science (80-.).*, vol. 334, no. 6058, pp. 928–935, 2011, doi: 10.1126/science.1212741.

[19] Cadex Electronics, "BU-104a: Comparing the Battery with other Power Sources," *Battery University*, 2015. http://batteryuniversity.com/learn/article/comparing_the_battery_with_other_power_sources (accessed Feb. 07, 2021).

[20] G. Z. Chen, "Supercapacitor and supercapattery as emerging electrochemical energy stores," *Int. Mater. Rev.*, vol. 62, no. 4, pp. 173–202, 2017, doi: 10.1080/09506608.2016.1240914.

[21] G. Zubi, R. Dufo-López, M. Carvalho, and G. Pasaoglu, "The lithium-ion battery: State of the art and future perspectives," *Renew. Sustain. Energy Rev.*, vol. 89, no. March, pp. 292–308, 2018, doi: 10.1016/j.rser.2018.03.002.

[22] D. L. Thompson *et al.*, "The importance of design in lithium ion battery recycling-a critical review,"

Green Chem., vol. 22, no. 22, pp. 7585–7603, 2020, doi: 10.1039/d0gc02745f.
[23] World Economic Forum; Global Battery Alliance, "A Vision for a Sustainable Battery Value Chain in 2030 Unlocking the Full Potential to Power Sustainable Development and Climate Change Mitigation including photocopying and recording, or by any information storage and retrieval system. 3 A Vision for a S," no. September, 2019, [Online]. Available: www.weforum.org.
[24] "BU-209: How does a Supercapacitor Work?" https://batteryuniversity.com/learn/article/whats_the_role_of_the_supercapacitor (accessed Dec. 19, 2020).
[25] P. J. Hall and E. J. Bain, "Energy-storage technologies and electricity generation," *Energy Policy*, vol. 36, no. 12, pp. 4352–4355, 2008, doi: 10.1016/j.enpol.2008.09.037.
[26] K. Jayaramulu *et al.*, "Covalent Graphene-MOF Hybrids for High-Performance Asymmetric Supercapacitors," *Adv. Mater.*, vol. 2004560, 2020, doi: 10.1002/adma.202004560.
[27] M. R. Lukatskaya, B. Dunn, and Y. Gogotsi, "Multidimensional materials and device architectures for future hybrid energy storage," *Nat. Commun.*, vol. 7, pp. 1–13, 2016, doi: 10.1038/ncomms12647.
[28] C. Toth and L. Elek, *Materials for Sustainable Energy- A Collection of Peer-Reviewed Research and Review Articles from Nature Publishing Group*, vol. 22, no. 3. 2011.
[29] Kush Kumar Upadhyay, "Metal Oxides and Sulfides based materials active in negative potential window for Supercapacitors," 2018.
[30] S. Cheng, "Effect of aluminum foil etching process on graphene super capacitor," *Chem. Eng. Trans.*, vol. 46, pp. 655–660, 2015, doi: 10.3303/CET1546110.
[31] P. Kurzweil, *Electrochemical Double-layer Capacitors*. Elsevier B.V., 2015.
[32] Francois Beguin, *Supercapacitors: Materials, Systems, and Applications*. 2013.
[33] T. Brousse, D. Bélanger, and J. W. Long, "To Be or Not To Be Pseudocapacitive?," *J. Electrochem. Soc.*, vol. 162, no. 5, pp. A5185–A5189, 2015, doi: 10.1149/2.0201505jes.
[34] N. R. Chodankar *et al.*, "True Meaning of Pseudocapacitors and Their Performance Metrics: Asymmetric versus Hybrid Supercapacitors," *Small*, vol. 16, no. 37, pp. 1–35, 2020, doi: 10.1002/smll.202002806.
[35] S. Li, J. Chen, J. Xiong, X. Gong, J. Ciou, and P. S. Lee, "Encapsulation of MnS Nanocrystals into N, S-Co-doped Carbon as Anode Material for Full Cell Sodium-Ion Capacitors," *Nano-Micro Lett.*, vol. 12, no. 1, 2020, doi: 10.1007/s40820-020-0367-9.
[36] J. Muzaffar, Aqib Ahamed, M. Basheer Deshmukh, Kalim Thirumalai, "A review on recent advances in hybrid supercapacitors: Design, fabrication and applications," *Renew. Sustain. Energy Rev.*, vol. 101, 2019, doi: 10.1016/j.rser.2018.10.026.
[37] "How are hybrid supercapacitors different than traditional supercapacitor (EDLC)?" https://www.eaton.com/us/en-us/products/electronic-components/faq/what-is-a-hybrid-supercapacitor.html (accessed Feb. 08, 2021).
[38] B. Viswanathan, *Energy Sources: Fundamentals of Chemical Conversion Processes and Applications*. 2016.
[39] J. Libich, J. Máca, J. Vondrák, O. Čech, and M. Sedlaříková, "Supercapacitors: Properties and applications," *J. Energy Storage*, vol. 17, no. March, pp. 224–227, 2018, doi: 10.1016/j.est.2018.03.012.
[40] J. Cherusseri, D. Pandey, and J. Thomas, "Symmetric, Asymmetric, and Battery-Type Supercapacitors Using Two-Dimensional Nanomaterials and Composites," *Batter. Supercaps*, vol. 3, no. 9, pp. 860–875, 2020, doi: 10.1002/batt.201900230.
[41] W. G. Pell and B. E. Conway, "Peculiarities and requirements of asymmetric capacitor devices based on combination of capacitor and battery-type electrodes," *J. Power Sources*, vol. 136, no. 2 SPEC. ISS., pp. 334–345, 2004, doi: 10.1016/j.jpowsour.2004.03.021.
[42] N. Choudhary *et al.*, "Asymmetric Supercapacitor Electrodes and Devices," *Adv. Mater.*, vol. 29, no. 21, 2017, doi: 10.1002/adma.201605336.
[43] H. Jeon, I. Cho, H. Jo, K. Kim, M. H. Ryou, and Y. M. Lee, "Highly rough copper current collector: Improving adhesion property between a silicon electrode and current collector for flexible lithium-ion batteries," *RSC Adv.*, vol. 7, no. 57, pp. 35681–35686, 2017, doi: 10.1039/c7ra04598k.
[44] Y. Huang *et al.*, "Hierarchically Mesostructured Aluminum Current Collector for Enhancing the Performance of Supercapacitors," *ACS Appl. Mater. Interfaces*, vol. 10, no. 19, pp. 16572–16580, 2018, doi: 10.1021/acsami.8b03647.
[45] L. Liu, H. Zhao, Y. Wang, Y. Fang, J. Xie, and Y. Lei, "Evaluating the Role of Nanostructured Current Collectors in Energy Storage Capability of Supercapacitor Electrodes with Thick Electroactive

Materials Layers," *Adv. Funct. Mater.*, vol. 28, no. 6, pp. 1–9, 2018, doi: 10.1002/adfm.201705107.
[46] S. Wennig *et al.*, "The influence of different pre-treatments of current collectors and variation of the binders on the performance of Li4Ti5O12 anodes for lithium ion batteries," *J. Appl. Electrochem.*, vol. 45, no. 10, pp. 1043–1055, 2015, doi: 10.1007/s10800-015-0878-0.
[47] Kamal K. Kar, *Handbook of Nanocomposite Supercapacitor Materials I*. Springer Series in Materials Science300, 2020.
[48] H. Luo, J. Zhu, E. Sahraei, and Y. Xia, "Adhesion strength of the cathode in lithium-ion batteries under combined tension/shear loadings," *RSC Adv.*, vol. 8, no. 8, pp. 3996–4005, 2018, doi: 10.1039/c7ra12382e.
[49] N. A. Salleh, S. Kheawhom, and A. A. Mohamad, "Characterizations of nickel mesh and nickel foam current collectors for supercapacitor application," *Arab. J. Chem.*, vol. 13, no. 8, pp. 6838–6846, 2020, doi: 10.1016/j.arabjc.2020.06.036.
[50] C. Portet, P. L. Taberna, P. Simon, and C. Laberty-Robert, "Modification of Al current collector surface by sol-gel deposit for carbon-carbon supercapacitor applications," *Electrochim. Acta*, vol. 49, no. 6, pp. 905–912, 2004, doi: 10.1016/j.electacta.2003.09.043.
[51] D. Mata *et al.*, "Wet-etched Ni foils as active catalysts towards carbon nanofiber growth," *Carbon N. Y.*, vol. 48, no. 10, pp. 2839–2854, 2010, doi: 10.1016/j.carbon.2010.04.016.
[52] I. Bispo-Fonseca, J. Aggar, C. Sarrazin, P. Simon, and J. F. Fauvarque, "Possible improvements in making carbon electrodes for organic supercapacitors," *J. Power Sources*, vol. 79, no. 2, pp. 238–241, 1999, doi: 10.1016/S0378-7753(99)00175-5.
[53] G. F. Yang, K. Y. Song, and S. K. Joo, "A metal foam as a current collector for high power and high capacity lithium iron phosphate batteries," *J. Mater. Chem. A*, vol. 2, no. 46, pp. 19648–19652, 2014, doi: 10.1039/c4ta03890h.
[54] G. H. An, S. N. Cha, and H. J. Ahn, "Surface functionalization of the terraced surface-based current collector for a supercapacitor with an improved energy storage performance," *Appl. Surf. Sci.*, vol. 478, no. May 2018, pp. 435–440, 2019, doi: 10.1016/j.apsusc.2019.01.280.
[55] N. Bellakhal and J. L. Brisset, "Oxygen plasma preparation of nickel oxide layers," *J. Chem. Res. - Part S*, no. 6, pp. 238–239, 2001, doi: 10.3184/030823401103169612.
[56] "Dry Etching and Wet Etching." https://www.thierry-corp.com/plasma-knowledgebase/dry-etching-and-wet-etching (accessed Feb. 10, 2021).
[57] C. Norvell J. Nelson, Palo Alto, "NICKEL ETCHING PROCESS AND SOLUTION," 1985.
[58] "Handbook_of_Metal_Etchants.pdf.part." .
[59] M. P. Materials, "Wet-Chemical Etching of Metals," p. 7, [Online]. Available: www.microchemicals.com/downloads/application_notes.html.
[60] P. Zhu, D. Gastol, J. Marshall, R. Sommerville, V. Goodship, and E. Kendrick, "A review of current collectors for lithium-ion batteries," *J. Power Sources*, vol. 485, no. November 2020, p. 229321, 2021, doi: 10.1016/j.jpowsour.2020.229321.
[61] P. Giannakou, M. G. Masteghin, R. C. T. Slade, S. J. Hinder, and M. Shkunov, "Energy storage on demand: Ultra-high-rate and high-energy-density inkjet-printed NiO micro-supercapacitors," *J. Mater. Chem. A*, vol. 7, no. 37, pp. 21496–21506, 2019, doi: 10.1039/c9ta07878a.
[62] Y. Z. Zhang *et al.*, "Printed supercapacitors: Materials, printing and applications," *Chem. Soc. Rev.*, vol. 48, no. 12, pp. 3229–3264, 2019, doi: 10.1039/c7cs00819h.
[63] T. Choi, S. J. Kim, S. Park, T. Y. Hwang, Y. Jeon, and B. H. Hong, "Roll-to-roll continuous patterning and transfer of graphene via dispersive adhesion," *Nanoscale*, vol. 7, no. 16, pp. 7138–7142, 2015, doi: 10.1039/c4nr06991a.
[64] D. Yu *et al.*, "Roll-to-roll manufacturing of micropatterned adhesives by template compression," *Materials (Basel).*, vol. 12, no. 1, pp. 1–12, 2018, doi: 10.3390/ma12010097.
[65] L. Pereira, "Microelectrónica I_Etching," *Acetatos de Microelectrónica I*. pp. 3, 4, 18–26, 31, 2018.
[66] "Dry Etching Recipes." https://wiki.nanotech.ucsb.edu/wiki/Dry_Etching_Recipes (accessed Feb. 16, 2021).
[67] J. M. Baptista, J. S. Sagu, U. W. KG, and K. Lobato, "State-of-the-art materials for high power and high energy supercapacitors: Performance metrics and obstacles for the transition from lab to industrial scale – A critical approach," *Chem. Eng. J.*, vol. 374, no. February, pp. 1153–1179, 2019, doi: 10.1016/j.cej.2019.05.207.
[68] R. White, "Aqua Regia Etch Standard Operating Procedure Faculty Supervisor: Prof. Robert White, Mechanical Engineering (x72210) Safety Office: Peter Nowak x73246 (Just dial this directly on any campus phone.) (617)627-3246 (From off-campus or from a cell phone) Tuft," vol. 73246, no. 617, pp.

3–6, 2017, [Online]. Available: http://engineering.tufts.edu/microfab/documents/SOP_AquaRegiaEtch.pdf.
[69] A. Regia, "Standard Operating Procedure AQUA REGIA," pp. 3–5, 2018, [Online]. Available: http://ehs.yale.edu/PPEPolicy.
[70] F. Bonilla, "Aqua Regia and Base Metals," vol. 4, no. 1, pp. 128–130.
[71] J. H. Seo, J.-H. Ryu, and D. N. Lee, "Formation of Crystallographic Etch Pits during AC Etching of Aluminum," *J. Electrochem. Soc.*, vol. 150, no. 9, p. B433, 2003, doi: 10.1149/1.1596952.
[72] J. Shen, Y. Chen, F. Zhang, D. Zhang, and Y. Gan, "Morphological and crystallographic evolution of patterned silicon substrate etched in TMAH solutions," *Appl. Surf. Sci.*, vol. 496, no. August, p. 143720, 2019, doi: 10.1016/j.apsusc.2019.143720.
[73] N. O. This, P. Setup, S. Preparation, and P. Always, "Nickel etch using Nickel etch using," pp. 2–4.
[74] "Iron(III) chloride." https://ceramica.fandom.com/wiki/Iron(III)_chloride.
[75] D. M. Allen and H. J. A. Almond, "Characterisation of aqueous ferric chloride etchants used in industrial photochemical machining," *J. Mater. Process. Technol.*, vol. 149, no. 1–3, pp. 238–245, 2004, doi: 10.1016/j.jmatprotec.2004.02.044.
[76] X. Sang, E. Chen, and J. P. Chang, "Patterning nickel for extreme ultraviolet lithography mask application I. Atomic layer etch processing," *J. Vac. Sci. Technol. A*, vol. 38, no. 4, p. 042603, 2020, doi: 10.1116/6.0000190.
[77] M. M. Vadiyar *et al.*, "Contact angle measurements: A preliminary diagnostic tool for evaluating the performance of ZnFe2O4 nano-flake based supercapacitors," *Chem. Commun.*, vol. 52, no. 12, pp. 2557–2560, 2016, doi: 10.1039/c5cc08373g.
[78] "Adhesion and Surface Energy," *henniker plasma*. https://plasmatreatment.co.uk/pt/plasma-technology-overview/adhesion-and-surface-energy (accessed Mar. 15, 2021).
[79] B. N. Sahoo, B. Kandasubramanian, and A. Thomas, " Effect of TiO 2 Powder on the Surface Morphology of Micro/Nanoporous Structured Hydrophobic Fluoropolymer Based Composite Material ," *J. Polym.*, vol. 2013, pp. 1–4, 2013, doi: 10.1155/2013/615045.
[80] A. Shafaamri *et al.*, "Effects of TiO2 Nanoparticles on the Overall Performance and Corrosion Protection Ability of Neat Epoxy and PDMS Modified Epoxy Coating Systems," *Front. Mater.*, vol. 6, no. January, pp. 1–19, 2020, doi: 10.3389/fmats.2019.00336.
[81] B. A. Mei, O. Munteshari, J. Lau, B. Dunn, and L. Pilon, "Physical Interpretations of Nyquist Plots for EDLC Electrodes and Devices," *J. Phys. Chem. C*, vol. 122, no. 1, pp. 194–206, 2018, doi: 10.1021/acs.jpcc.7b10582.
[82] H. Guo *et al.*, "Active carbon electrode fabricated via large-scale coating-transfer process for high-performance supercapacitor," *Appl. Phys. A Mater. Sci. Process.*, vol. 123, no. 7, 2017, doi: 10.1007/s00339-017-1069-0.
[83] A. Area, "Application Area : Fundamental EIS Data fitting – How to obtain good starting values of equivalent circuit elements."
[84] Gramy Instruments Inc., "Basics of Electrochemical Impedance Spectroscopy Impedance Values," *Appl. Note Rev. 2.0*, no. 215, pp. 1–28, 2014.
[85] A. Laheäär, P. Przygocki, Q. Abbas, and F. Béguin, "Appropriate methods for evaluating the efficiency and capacitive behavior of different types of supercapacitors," *Electrochem. commun.*, vol. 60, pp. 21–25, 2015, doi: 10.1016/j.elecom.2015.07.022.
[86] M. Rajkumar, C. T. Hsu, T. H. Wu, M. G. Chen, and C. C. Hu, "Advanced materials for aqueous supercapacitors in the asymmetric design," *Prog. Nat. Sci. Mater. Int.*, vol. 25, no. 6, pp. 527–544, 2015, doi: 10.1016/j.pnsc.2015.11.012.
[87] X. Sang, E. Chen, and J. P. Chang, "Patterning nickel for extreme ultraviolet lithography mask application I. Atomic layer etch processing," *J. Vac. Sci. Technol. A*, vol. 38, no. 4, p. 042603, 2020, doi: 10.1116/6.0000190.
[88] O. Näth, A. Stephen, J. Rösler, and F. Vollertsen, "Structuring of nanoporous nickel-based superalloy membranes via laser etching," *J. Mater. Process. Technol.*, vol. 209, no. 10, pp. 4739–4743, 2009, doi: 10.1016/j.jmatprotec.2008.11.042.
[89] Y. Huang *et al.*, "Hierarchically Mesostructured Aluminum Current Collector for Enhancing the Performance of Supercapacitors," *ACS Appl. Mater. Interfaces*, vol. 10, no. 19, pp. 16572–16580, 2018, doi: 10.1021/acsami.8b03647.
[90] S. M. Lee *et al.*, "Evaluation of the waterproof ability of a hydrophobic nickel micromesh with array-type microholes," *J. Micromechanics Microengineering*, vol. 19, no. 12, 2009, doi: 10.1088/0960-1317/19/12/125024.

[91] K. Yoo *et al.*, “Direct physical exfoliation of few-layer graphene from graphite grown on a nickel foil using polydimethylsiloxane with tunable elasticity and adhesion,” *Nanotechnology*, vol. 24, no. 20, 2013, doi: 10.1088/0957-4484/24/20/205302.
[92] J. H. Lee, H. G. Kim, G. S. Khang, H. B. Lee, and M. S. Jhon, “Characterization of wettability gradient surfaces prepared by corona discharge treatment,” *J. Colloid Interface Sci.*, vol. 151, no. 2, pp. 563–570, 1992, doi: 10.1016/0021-9797(92)90504-F.
[93] J. Izdebska, *Corona Treatment*, no. 2014. Elsevier Inc., 2015.
[94] C. P. Yang, Y. X. Yin, S. F. Zhang, N. W. Li, and Y. G. Guo, “Accommodating lithium into 3D current collectors with a submicron skeleton towards long-life lithium metal anodes,” *Nat. Commun.*, vol. 6, no. May, pp. 1–9, 2015, doi: 10.1038/ncomms9058.

MATERIALS

In this section, a list of the reagents used for this work is presented.

Table 14- Reagents used in this work, with abbreviation, purity, CAS and company.

Material	***Abbreviation***	***Purity***	***CAS***	***Company***
Hydrochloric acid	HCl	37%	7647-01-0	Carl Roth
Nitric acid	HNO_3	>60%	7697-37-2	José Manuel Gomes dos Santos, Lda
Sulfuric acid	H_2SO_4	96%	7664-93-9	José Manuel Gomes dos Santos, Lda
Hydrogen peroxide	H_2O_2	-	7722-84-1	José Manuel Gomes dos Santos, Lda
Iron Chloride	$FeCl_3$	≥98,5%,	7705-08-0	Carl Roth
Potassium hydroxide	KOH	85%	1310-58-3	Chemlab
Ethanol	C_2H_5OH	96%	64-17-5	José Manuel Gomes dos Santos, Lda
Acetone	C_3H_6O	99.6%	67-64-1	José Manuel Gomes dos Santos, Lda

OPTICAL MICROSCOPE

The images obtained were used to infer if the resin was well printed onto the foil using the optical microscope (Olympus BX51) with the bellow described magnifications.

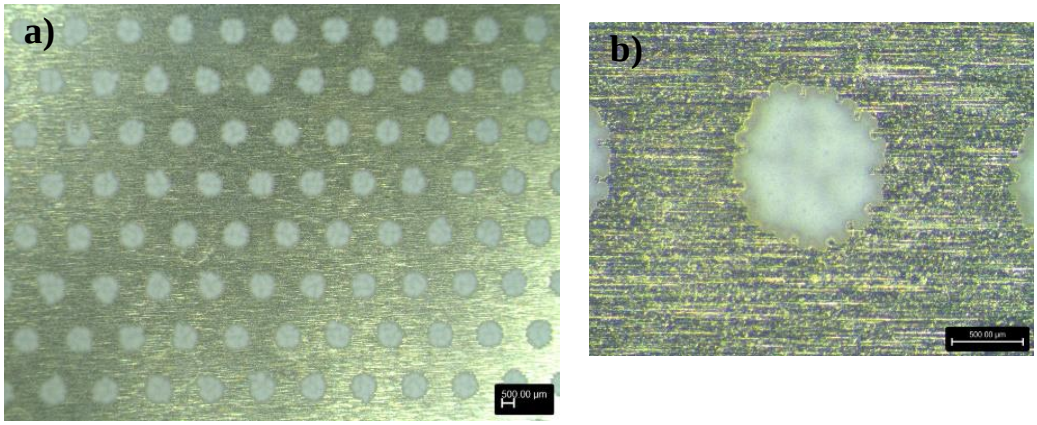

Figure 27- Optical microscope images of screen-printing sample before etching at a magnification of a)500 µm and b) 500 µm.

CROSS-CUT TEST

The standard classification to evaluate the adhesion of the electrodes according to the ISO standards is showed.

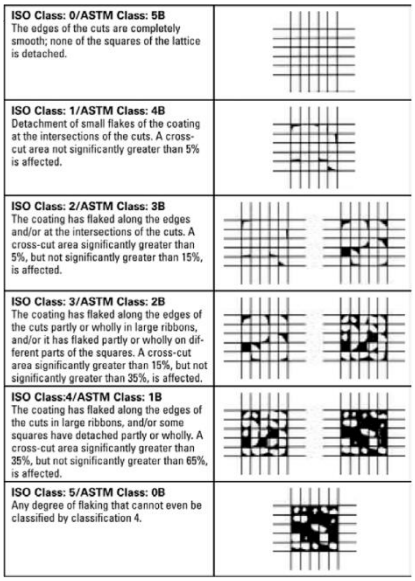

Figure 28-Standard ISO classification for adhesion strength.

IMAGE J

The SEM images used to calculate the average portrusions size with *Imagej* are displayned in this section.

a)

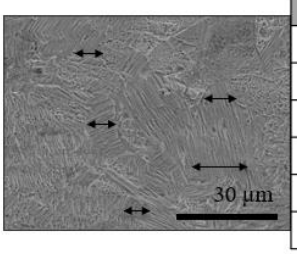

Pores size (µm)
5.5
7.5
5.7
9.5
7.3
Average = 7.1

b)

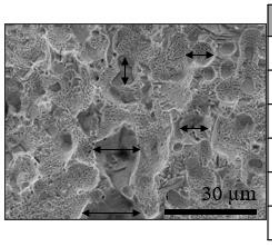

Pores size (µm)
14
9.1
18.7
9.7
9.4
Average = 12.2

c)

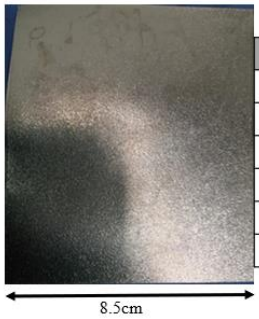

Pores size (µm)
456.9
783.3
391.65
393.01
490.6
Average = 503

Figure 29- ImageJ measurements of avergae pore size for a)$FeCl_3$ - best conditions; b)$H_2SO_4/H_2O_2/H_2O$ - best conditions and c)Calendared sample.

PHYSICAL CHARACTERIZATION -EDS

In the following figures, the EDS analysis of the different etched CCs are showed.

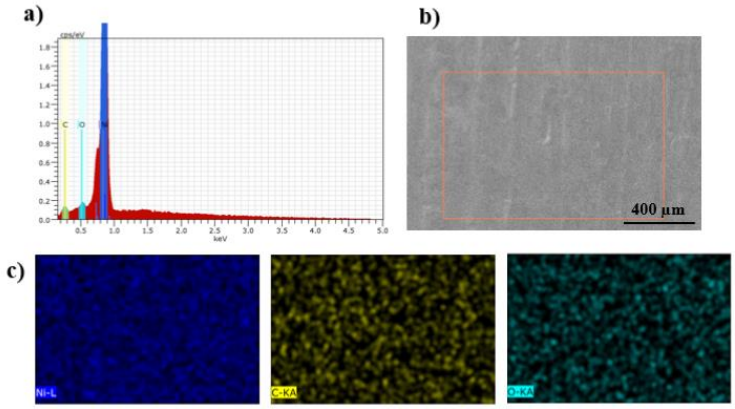

Figure 30- EDS test performed on the Argon etched CC. a) EDS spectrum, b) EDS layered image, c) EDS elemental mapping.

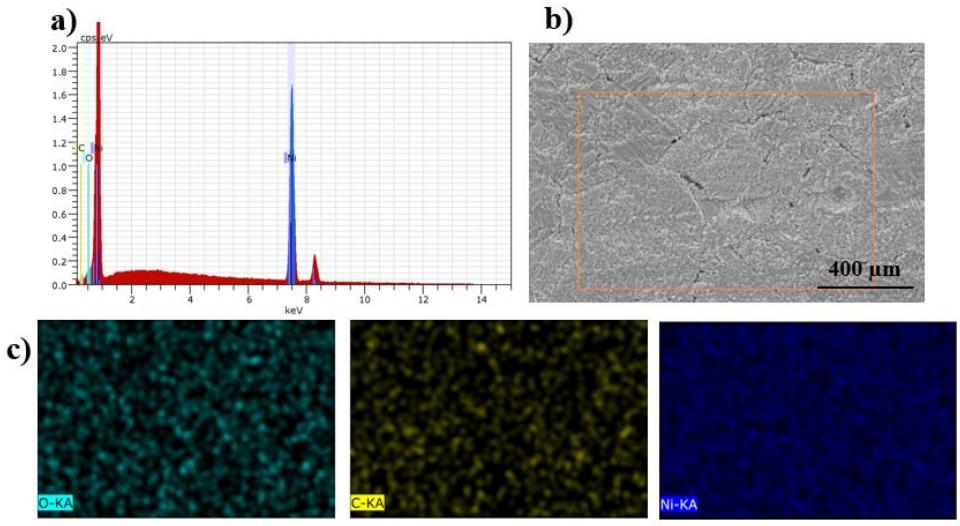

Figure 31- EDS test performed on the chemical ($H_2SO_4/H_2O_2/H_2O$ for 10 minutes) and Argon etched CC. a) EDS spectrum, b) EDS layered image, c) EDS elemental mapping.

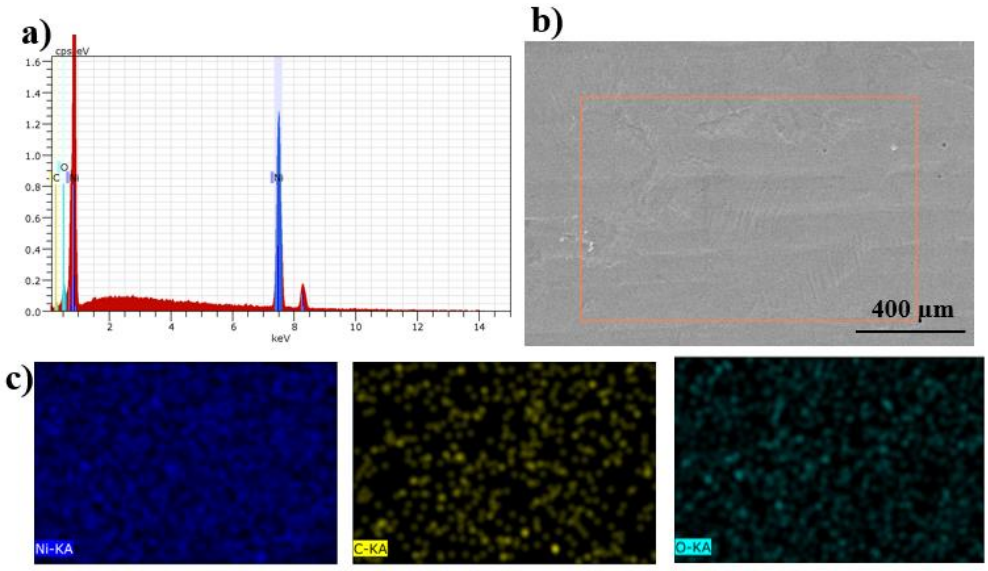

Figure 32- - EDS test performed on the O_2 etched CC. a) EDS spectrum, b) EDS layered image, c) EDS elemental mapping.

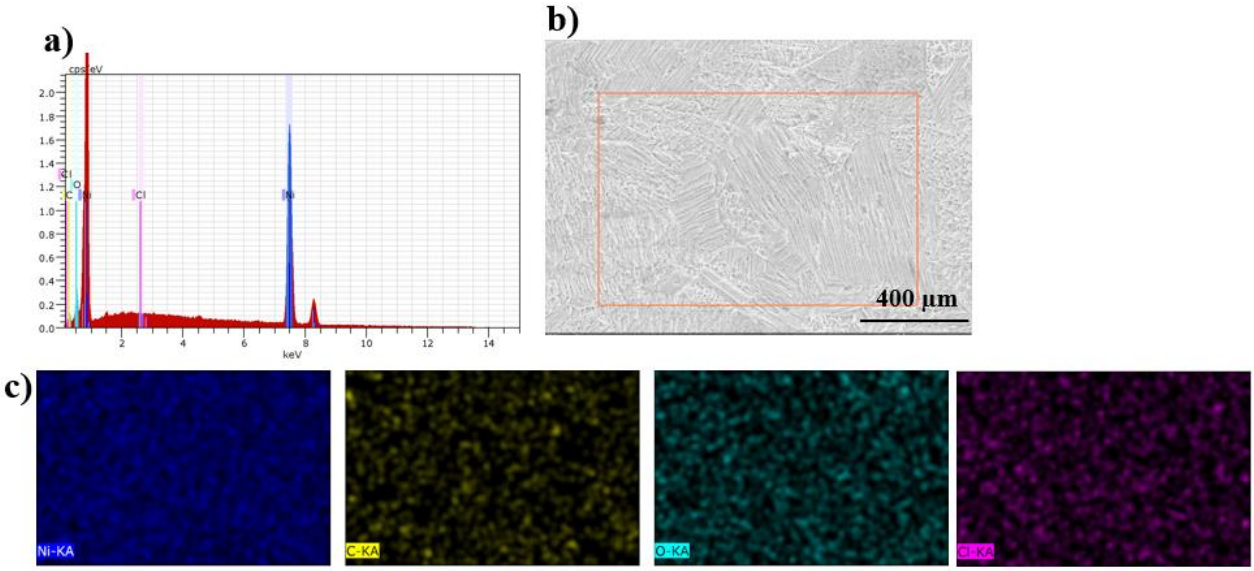

Figure 34- EDS test performed on the chemical ($H_2SO_4/H_2O_2/H_2O$ for 10 minutes) and O_2 etched CC. a) EDS spectrum, b) EDS layered image, c) EDS elemental mapping.

ELETROCHEMICAL ANALYSIS

Both cyclic voltametry and EIS analysis was performed on the different etchant solutions at the different emploted times.Here, these results are presented.

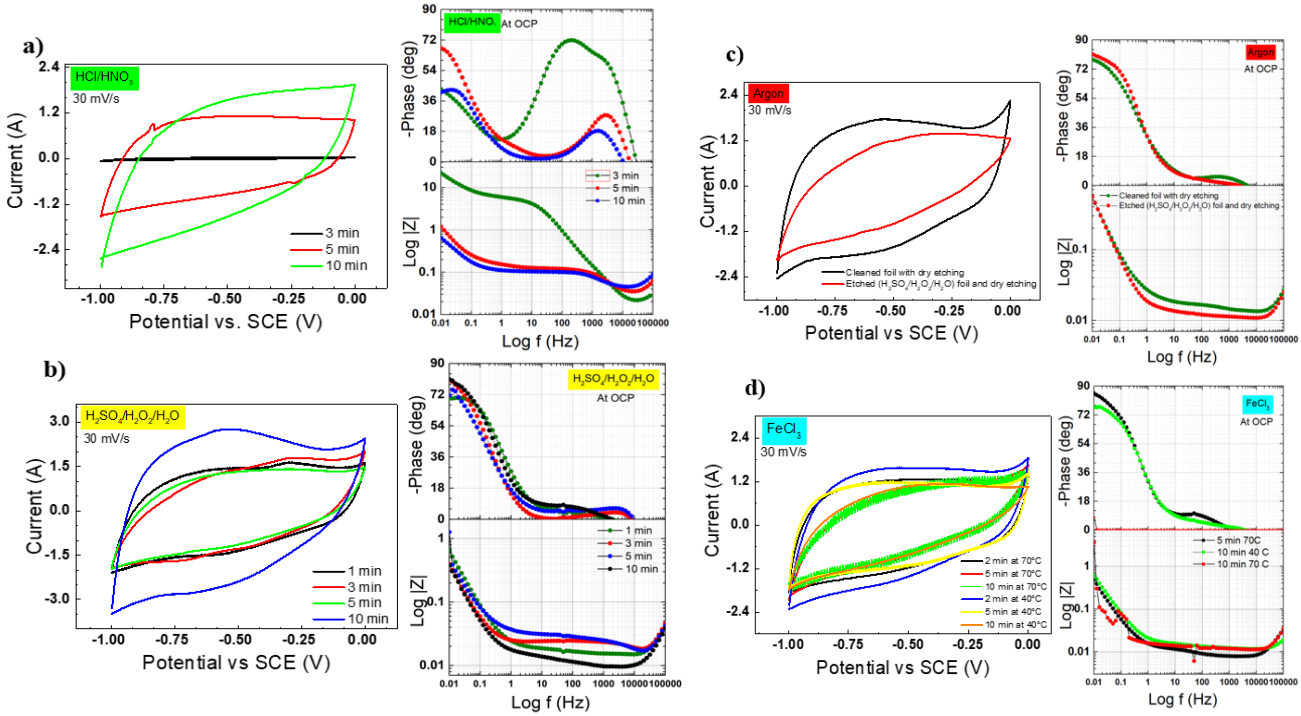

Figure 35- Cyclic voltammetry and bode por for a) HCl/HNO_3 etched CC at different times, b) $H_2SO_4/H_2O_2/H_2O$ etched CC at different times, c) Argon etched CC, d) $FeCl_3$ etched CC at different times and temperature.

Figure 36 shows the bode plot referent to the best conditions of the FeCl3 etching and its comparison with the screen-printing etched CC.

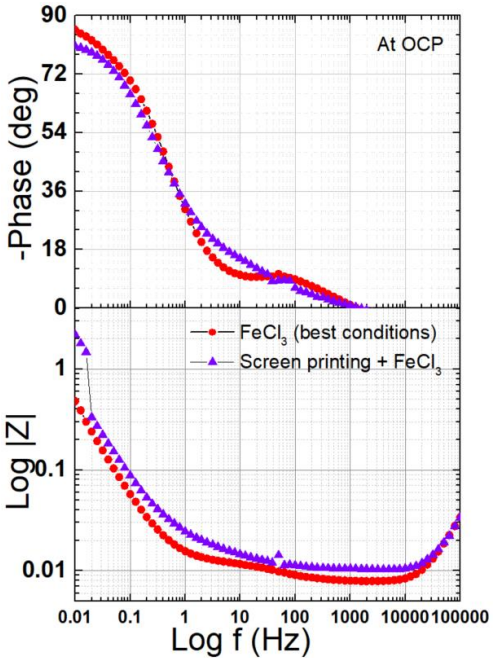

Figure 36- Bode plot on $FeCl_3$ etched CC and screen-printing + $FeCl_3$ ethched CC.

Cyclic voltammetry at different scan rates for the cleaned and calendared CC is also showed.

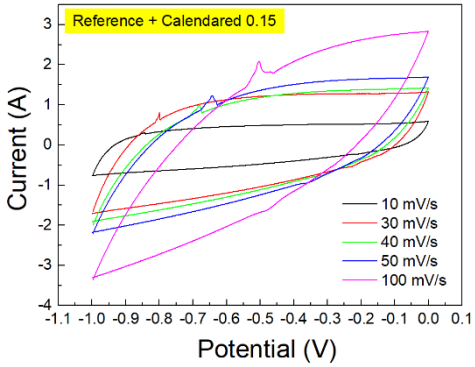

Figure 37- Cyclic voltametry at different scan rates for calendared CC at 0.15mm.

Here, the Nyquist plot comparison for before and after the aggressive test is showed.

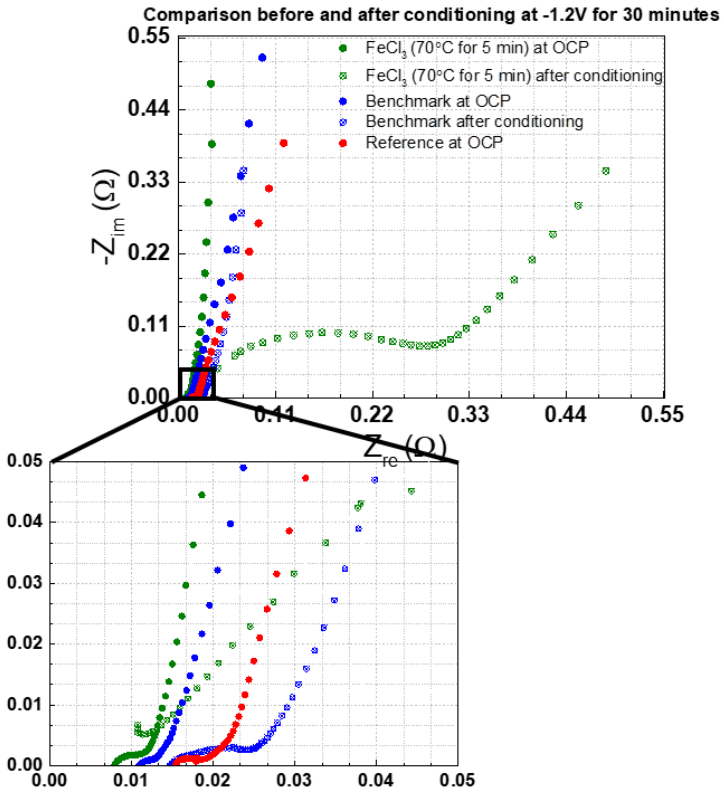

Figure 38- Nyquist plot for reference, benhcmark and $FeCl_3$ (70°C for 5 minutes) before and after conditiong at -1.2V for 30 minutes.

The capacitance and coulombc eficciency test for the $H_2SO_4/H_2O_2/H_2O$ for 10 minutes etched CC and HCL/HNO_3 for 10 minutes etched CC is showed.

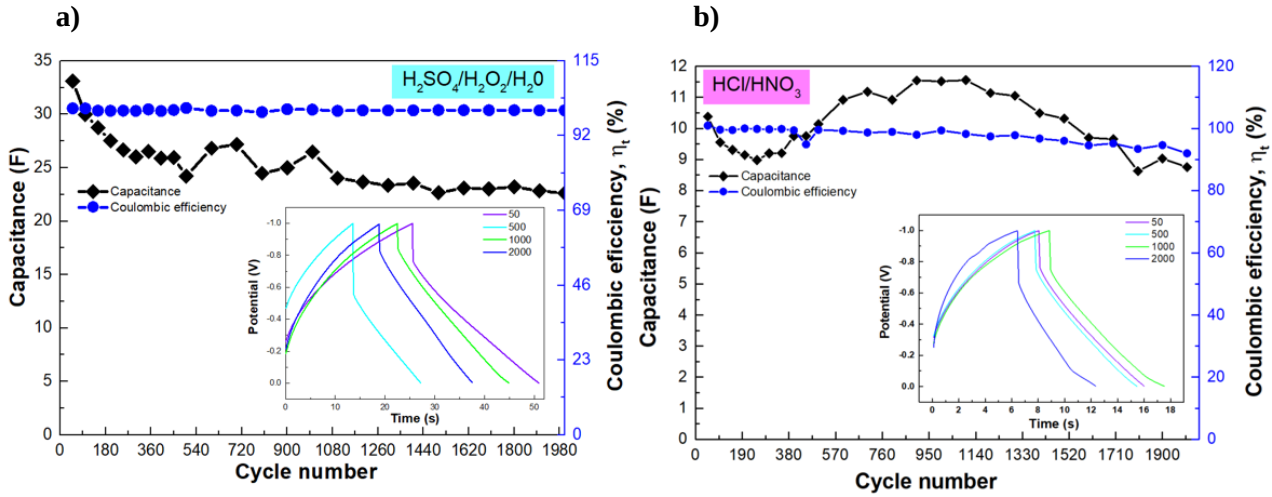

Figure 39- Capacitance and coulombic efficiency for a) $H_2SO_4/H_2O_2/H_2O$ (10 minutes) etched CC and b) HCl/HNO_3 (10 minutes) etched CC.